

---

# Recurrent neural networks: vanishing and exploding gradients are not the end of the story

---

**Nicolas Zucchet**

Department of Computer Science  
ETH Zürich  
nzucchet@ethz.ch

**Antonio Orvieto**

ELLIS Institute Tübingen  
MPI for Intelligent Systems  
Tübingen AI Center  
antonio@tue.ellis.eu

## Abstract

Recurrent neural networks (RNNs) notoriously struggle to learn long-term memories, primarily due to vanishing and exploding gradients. The recent success of state-space models (SSMs), a subclass of RNNs, to overcome such difficulties challenges our theoretical understanding. In this paper, we delve into the optimization challenges of RNNs and discover that, as the memory of a network increases, changes in its parameters result in increasingly large output variations, making gradient-based learning highly sensitive, even without exploding gradients. Our analysis further reveals the importance of the element-wise recurrence design pattern combined with careful parametrizations in mitigating this effect. This feature is present in SSMs, as well as in other architectures, such as LSTMs. Overall, our insights provide a new explanation for some of the difficulties in gradient-based learning of RNNs and why some architectures perform better than others.

Recurrent neural networks [RNNs; 1, 2] have long been the canonical architecture for modeling temporal data [3, 4]. However, they are notoriously difficult to train on long sequences, as error signals flowing backward in time tend to either vanish or explode [5–8]. Attention mechanisms [9], as featured in transformers [10], address these issues by enabling direct token-to-token communication, considerably simplifying signal propagation across long time intervals. Yet, their superior performance comes with increased computational and memory costs, due to their quadratic scaling in the sequence length. This limitation has motivated significant research aimed at making transformers more efficient [11–15].

A promising line of research in this direction involves a new type of linear recurrent networks known as state-space models [SSMs; 16–22]. These models trade expressivity for faster training speed, and they have been shown to be particularly effective at capturing long-range dependencies. In this paper, we wonder whether this effectiveness can be solely attributed to their ability to avoid vanishing and exploding gradients. The simplicity of such models presents an opportunity for in-depth theoretical analysis. We focus on signal propagation within these models.

After reviewing classical results on recurrent neural networks in Section 1, we demonstrate that they can suffer an understudied problem: the curse of memory (Section 2). As the recurrent network encodes longer memories, the network’s activity becomes increasingly sensitive to changes in its parameters, even when its dynamics remains stable. In Section 3, we then show that SSMs, as well as other architectures such as LSTMs, are well equipped to mitigate this issue. We conclude our study by analyzing a simple teacher-student task, which already reveals the remarkable complexity underlying the learning of linear recurrent networks (Section 4). Finally, we discuss how our findings extend to more realistic scenarios (Section 5). Overall, our results reveal that vanishing and exploding gradients are not the end of the story and that there exists an additional layer of complexity beyond them.

## 1 Vanishing and exploding gradients

Let us first introduce the notations we will be using throughout the rest of the paper. We consider a recurrent neural network with hidden state  $h_t$ , update function  $f_\theta$  parametrized by  $\theta$ , and input sequence  $(x_t)_t$ . The average performance of the network is measured by a loss  $L$ . We have

$$h_{t+1} = f_\theta(h_t, x_{t+1}) \text{ and } L = \mathbb{E} \left[ \sum_{t=1}^T L_t(h_t) \right]. \quad (1)$$

The gradient of the instantaneous loss  $L_t$  with respect to the parameters  $\theta$  is then equal to

$$\frac{dL_t}{d\theta} = \frac{\partial L_t}{\partial h_t} \frac{dh_t}{d\theta} = \frac{\partial L_t}{\partial h_t} \sum_{t' \leq t} \frac{dh_t}{dh_{t'}} \frac{\partial f_\theta}{\partial \theta}(h_{t'-1}, x_{t'}) \quad (2)$$

In the equation above, we used  $\partial$  to denote partial derivatives and  $d$  for total derivatives. Using this notation enables us to distinguish between  $\partial_{h_t} L_t$ , which corresponds to the error backpropagated from the current loss term to the hidden state through the readout function, and  $d_{h_t} L$ , which accumulates the errors that are backpropagated through the future hidden state values. In particular,  $\partial_{h_t} L = \partial_{h_t} L_t$  and  $d_{h_t} L = \partial_{h_t} L_t(h_t) + \sum_{t' > t} d_{h_t} L_{t'}(h_{t'})$ . When stacking several recurrent layers on top of each other,  $\partial_{h_t} L$  corresponds to the current error being backpropagated propagated to the hidden state  $h_t$  through the hierarchy of the network and  $d_{h_t} L$  to future error signals backpropagated through the recurrence.

Early work [5] highlighted the difficulty for gradient descent to make recurrent neural networks remember past inputs that will later useful to produce a desired behavior. This is due to the fact that error signals flowing backward in time tend to either explode or vanish. The key quantity is

$$\frac{dh_t}{dh_{t'}} = \prod_{i=t'}^{t-1} \frac{\partial h_{i+1}}{\partial h_i} = \prod_{i=t'}^{t-1} \frac{\partial f_\theta}{\partial h}(h_i, x_{i+1}). \quad (3)$$

One can remark that this quantity exponentially converges to 0 when the spectral radius of the Jacobian  $\partial_h f_\theta$  is upper bounded by a constant strictly smaller than 1, and can exponentially explode if there exists some component bigger than 1. The error signal at time  $t$  backpropagated to time  $t'$  behaves similarly, as  $d_{h_{t'}} L_t = \partial_{h_t} L_t d_{h_t'} h_t$ . Gradient-based learning of long-term memories is thus difficult: the contribution of past hidden states to the current loss becomes either negligible or predominant as the time span considered increases.

Since then, the analysis has been refined [6–8] and the development of recurrent architectures has mostly been driven by the desire to solve this pathological issue. Most famously, the LSTM [3] unit, and later on the GRU [23], solve this problem by using memory neurons that facilitate direct information storage and retrieval, and by the same way error backpropagation. Other approaches to solving this problem, to name a few, involve gradient clipping [24, 8], activity normalization [25–27], careful weight initialization [28, 29] or enforcing architectural constraints such as hierarchical processing [30, 31], orthogonal weight matrices [32–34] and oscillations [35–37].

## 2 The curse of memory

According to common deep learning wisdom, it is often believed that solving the vanishing and exploding gradients problem enables recurrent neural networks to learn long-term dependencies. We challenge this view and question: is solving those issues really enough to ensure well-behaved loss landscapes? We answer negatively by showing that gradients can explode as the memory of the network increases, even when the dynamics of the network remains stable.

### 2.1 Intuition

Recurrent neural networks have something special: the very same update function  $f_\theta$  is applied over and over. Therefore, modifying the parameters  $\theta$  will not only influence one update, as changing the weights of a given layer in a feedforward neural network would, but all. As the memory of the network increases, the hidden states keep a trace of the effect of more updates. Hidden states thus become increasingly sensitive to parameter changes. This is the *curse of memory*. We borrow the

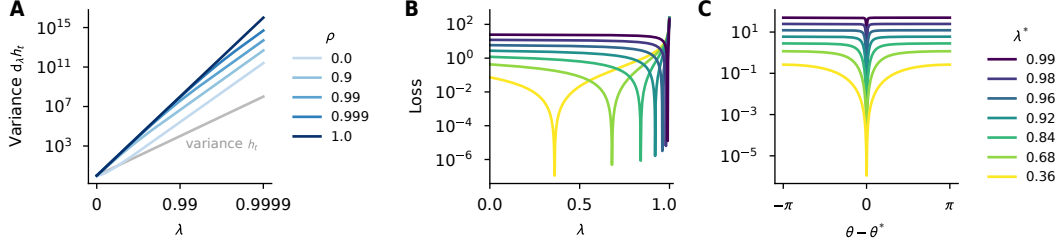


Figure 1: **Optimization of recurrent neural networks gets harder as their memory increases.** **A.** Evolution of the variance of  $d_\lambda h_t$  as a function of the recurrent parameter  $\lambda$  and of the input  $x$  auto-correlation decay rate  $\rho$ , when  $h_{t+1} = \lambda h_t + x_t$ . As the memory of the network increases ( $\lambda \rightarrow 1$ ),  $h_t$  becomes more sensitive to changes in  $\lambda$ , particularly as the elements in the input sequence become more correlated ( $\rho \rightarrow 1$ ). The explosion of  $d_\lambda h_t$  is faster than the one of  $h_t$ , as highlighted with the grey line obtained for  $\rho = 1$ . See Section 2.2 for more detail. **B.** **C.** Illustration of the phenomenon on the toy one-dimensional teacher-student task of Section 4.1, in which the teacher is parametrized by a real number  $\lambda^*$  and the student by a complex number  $\lambda$ . In **B.**,  $\lambda$  varies on the positive real axis and it varies on the circle of radius  $\lambda^*$  parametrized by  $\theta$  in **C.** The loss becomes sharper information is kept longer in memory, making gradient-based optimization nearly impossible.

term from [38, 39], and note that Martens and Sutskever [40] hypothesized that such a phenomenon could arise in RNNs and hinder their optimization.

Let us formalize our intuition and consider the sensitivity of the hidden state  $h_t$  on the parameters  $\theta$ :

$$\frac{dh_t}{d\theta} = \sum_{t' \leq t} \frac{dh_t}{dh_{t'}} \frac{\partial f_\theta}{\partial \theta}(h_{t'-1}, x_{t'}). \quad (4)$$

When information stays in the network’s memory for longer, the number of non-negligible Jacobian  $d_{h_{t'}} h_t$  terms increases. As a result, the magnitude of this sensitivity increases when the network encodes longer-term dependencies, and learning  $\theta$  becomes trickier. It is critical to note that this phenomenon arises even when exploding gradients are removed from the picture by constraining the eigenvalues of the recurrent Jacobian to be smaller than one and ensuring that the network dynamics remains stable. The rest of this section will be dedicated to studying quantitatively this behavior.

## 2.2 Signal propagation in linear diagonal recurrent neural networks

We study how hidden state and gradient magnitudes evolve as the network encodes longer-term dependencies. Ideally, we would like these quantities not to vanish or explode. This property improves the conditioning of the loss landscape [41] and hence eases optimization [42, 43]. We make the following assumptions:

- a) **Linear diagonal recurrent neural networks.** We restrict ourselves to update functions of the form  $f_\theta(h_t, x_{t+1}) = \lambda \odot h_t + x_{t+1}$  with  $\lambda$  a vector of the size of  $h_t$  and  $\odot$  the element-wise product. For ease of exposition, we present results for real-valued  $\lambda$  here; see Appendix A.2 for the complex-valued setting. While this assumption is strong, it allows us to identify some crucial mechanisms and it is satisfied for some models like S4 [17] and LRUs [20]. We later show our analysis can model some features of more sophisticated networks.
- b) **Infinite time horizon.** We consider infinite sequences and initialize the network dynamics at  $t_0 = -\infty$ . It simplifies our calculations while being a reasonable assumption when the sequences considered are longer than the characteristic timescales of the dependencies we want to learn.
- c) **Wide-sense stationarity.** We assume the different quantities that the network receives, which include the inputs  $x_t$ , to be wide-sense stationary (WSS). A random process  $X_t$  is said to be WSS if its auto-correlation function is independent of time, that is, for all  $t \in \mathbb{Z}$  and  $\Delta \in \mathbb{Z}$ ,  $\mathbb{E}_X [X_{t+\Delta} X_t] =: R_X(\Delta)$ , where  $\mathbb{E}_X$  denotes the expectation over the data. It corresponds to assuming that the statistics of the different sequences within the data are invariant to time shifts.

We are now equipped to analyze signal propagation in one recurrent layer, both in the forward and backward passes. We show that both hidden states and backpropagated errors explode as  $|\lambda| \rightarrow 1$ .

**Forward pass.** Here, we are interested in understanding how the hidden state variance  $\mathbb{E}[h_t^2]$  evolves as a function of the characteristic timescale of the network encoded in  $\lambda$  as well as the input auto-correlation function  $R_x$ . After a calculation that we defer to Appendix A.2, we obtain

$$\mathbb{E}[h_t^2] = \frac{1}{1 - \lambda^2} \left( R_x(0) + 2 \sum_{\Delta \geq 1} \lambda^\Delta R_x(\Delta) \right). \quad (5)$$

Importantly, the variance of the hidden state goes to infinity as longer-term dependencies are encoded within the network, that is  $|\lambda| \rightarrow 1$ . Additionally, the divergence speed depends on the input data distribution: it increases as consecutive time steps in the input distribution become more correlated (i.e., less of the  $R_x(\Delta)$  terms are negligible). This behavior already highlights potential difficulties of gradient-based learning of deep neural networks containing linear recurrent layers as the variance of neural activity can become arbitrarily large, hindering learning abilities of deeper layers.

**Backward pass.** Let us first derive the gradient of the loss with respect to  $\lambda$ . Using the chain rule we have  $d_\lambda L = \sum_t \partial_{h_t} L d_\lambda h_t$ . We thus seek to understand how  $d_\lambda h_t$  behaves. We remark that  $d_\lambda h_{t+1} = \lambda d_\lambda h_t + h_t$  so that  $d_\lambda h_t$  is a low pass filtered version of the hidden state, which is itself a low pass filter version of the inputs. It therefore comes as no surprise that the variance of  $d_\lambda h_t$  diverges faster than the one of  $h_t$  when  $|\lambda| \rightarrow 1$ . More precisely, we get

$$\mathbb{E} \left[ \left( \frac{dh_t}{d\lambda} \right)^2 \right] = \frac{1 + \lambda^2}{(1 - \lambda^2)^3} \left( R_x(0) + 2 \sum_{\Delta \geq 1} \lambda^\Delta R_x(\Delta) \right) + \frac{2}{(1 - \lambda^2)^2} \left( \sum_{\Delta \geq 1} \Delta \lambda^\Delta R_x(\Delta) \right). \quad (6)$$

We plot the exact behavior of this quantity when the auto-correlation of  $x$  satisfies  $R_x(\Delta) = \rho^{|\Delta|}$  on Figure 1 and refer the interested reader to the appendix for a derivation of Equation 6. Framed more generally, the hidden state of the network, and thus its final output, becomes increasingly sensitive to changes in recurrent parameters as the network reaches the edge of dynamical stability ( $|\lambda| \rightarrow 1$ ).

The last quantity that we need to consider is the error that is backpropagated to the inputs  $x$  of the recurrent layer. It can be observed that the backward pass is dual to the forward pass in the sense that it is a recurrent process that receives backpropagated errors  $\partial_{h_t} L$  and it runs in reverse time:

$$\frac{dL}{dx_t} = \frac{dL}{dh_t} \frac{\partial h_t}{\partial x_t} = \frac{dL}{dh_{t+1}} \frac{\partial h_{t+1}}{\partial h_t} + \frac{\partial L}{\partial h_t} = \lambda \frac{dL}{dh_{t+1}} + \frac{\partial L}{\partial h_t}, \quad (7)$$

in which we made use of  $\partial_{x_t} h_t = 1$ . It follows that the analysis we did for the forward pass also holds here. Crucially, this implies that the explosion behavior will be most significant for the recurrent parameters rather than for potential input or readout weights.

### 2.3 Extending the analysis to the non diagonal case

We now generalize our results to fully connected linear recurrent neural networks of the form  $h_{t+1} = Ah_t + x_t$ . For the sake of the analysis, we assume that  $A$  is complex diagonalizable, that is there exists a complex-valued matrix  $P$  and a complex-valued vector  $\lambda$  such that  $A = P \text{diag}(\lambda) P^{-1}$ . Note that this occurs with probability one under random initialization of  $A$  [20]. In this case,

$$h_t = Ph_t^{\text{diag}} \quad \text{with } h_{t+1}^{\text{diag}} = \text{diag}(\lambda) h_t^{\text{diag}} + P^{-1} x_{t+1} \quad (8)$$

and

$$\frac{dh_t}{dA} = \frac{\partial h_t}{\partial P} \frac{\partial P}{\partial A} + \frac{\partial h_t}{\partial h_t^{\text{diag}}} \frac{dh_t^{\text{diag}}}{d\lambda} \frac{\partial \lambda}{\partial A} + \frac{\partial h_t}{\partial h_t^{\text{diag}}} \frac{dh_t^{\text{diag}}}{dP^{-1}} \frac{\partial P^{-1}}{\partial A}. \quad (9)$$

From the previous analysis, we know that the dominating term in the limit  $|\lambda| \rightarrow 1$  among  $\partial_P h_t$ ,  $d_\lambda h_t$  and  $d_{P^{-1}} h_t$  is  $d_\lambda h_t$ , as  $P$  and  $P^{-1}$  act as readout and input weights. Given that all other terms do not directly depend on the magnitude of  $\lambda$ , we have that  $d_A h_t \simeq \partial_{h_t^{\text{diag}}} h_t d_\lambda h_t^{\text{diag}} \partial_A \lambda$ ; c.f. Appendix A.2.3 for formal statements. This has two consequences: First, the sensitivity of  $h_t$  on  $A$  will explode as longer memories are encoded and this directly comes from the eigenvalues of  $A$ . Second, as each entry of  $A$  typically impacts all eigenvalues of the matrix, the explosion behavior will be distributed across all entries, whereas it was concentrated on the eigenvalues for the diagonal case. We will later observe that this has significant practical consequences and partly explains why fully connected linear RNNs are difficult to train. As a side note, we remark that enforcing the matrix  $A$  to be orthogonal solves vanishing and exploding gradient issues but these weights may remain sensitive to learn because of the curse of memory.

### 3 Mitigating the curse of memory

We have discussed the sensitivity of recurrent networks to parameter updates. Given this problem, how can it be mitigated? Recurrent networks with diagonal connectivity are particularly well suited for this purpose. Besides enabling control over the Jacobian and avoiding exploding gradients, they facilitate the mitigation of the curse of memory. In this context, we demonstrate that state-space models and gated RNNs inherently incorporate such mechanisms.

#### 3.1 A solution: normalization and reparametrization

Both forward and backward passes explode as the network encodes longer memories. When  $h_{t+1} = \lambda h_t + x_{t+1}$ , we argue that it is decently easy to mitigate this effect. We aim to keep  $\mathbb{E}[h_t^2]$ ,  $\mathbb{E}[(d_\lambda h_t)^2]$  and  $\mathbb{E}[(d_{x_t} h_t)^2]$  independent of  $\lambda$ , similarly to initialization schemes ensuring the magnitude of neural activity remains constant in deep networks [44, 45] and independent of the layer width [42, 46, 43].

**Input normalization.** A simple way to enforce  $\mathbb{E}[h_t^2]$  to stay constant is to introduce a scaling factor  $\gamma(\lambda)$ , applied to the inputs a neuron receives, that satisfies  $\gamma(\lambda)^2 \mathbb{E}[h_t^2] = \Theta(1)$ . Given that the backward propagation of output errors to inputs is dual to the forward pass, the role of  $\gamma$  has in the backward pass will be similar. The value  $\gamma$  needs to take therefore both depends on the input distribution to normalize the forward pass, as well as on the output error distribution to normalize the backward pass. Perfect normalization is likely unrealistic, but some normalization can help, as shown in Figure 2.A.

**Eigenvalue reparametrization.** We are now left with keeping the gradient of the loss with respect to  $\lambda$  under control. Input normalization partly reduces the memory-induced exploding effect, but not entirely as the variance of  $d_\lambda h_t$  is much larger than the one of  $h_t$  (c.f. Fig.1.A). Reparametrization can close that gap. Indeed, if  $\lambda$  is parametrized by  $\omega$ , we have that  $d_\omega h_t = d_\lambda h_t d_\omega \lambda$ . Choosing a parameterization that is more and more granular as  $\lambda$  goes to 1 thus helps in keeping  $d_\omega h_t$  constant. Assuming  $\gamma$  is independent of  $\lambda$  for simplicity, achieving  $\mathbb{E}[(d_\omega h_t)^2] = \Theta(1)$  requires solving the differential equation  $\gamma(\lambda)^2 \lambda'(\omega)^2 \mathbb{E}[(d_\lambda h_t)^2] = 1$ . While deriving a universal optimal parameterization is again unrealistic due to dependency on the input distribution, reparametrization definitely helps, as shown in Figure 2.B. Figure 6 illustrates how it can affect the loss landscape.

**What about complex numbers?** We have not yet discussed the case  $\lambda \in \mathbb{C}$ , relevant for SSMs such as S4 [17]. We extend our analysis to complex  $\lambda$ s in Appendix A.3.2 and highlight that they are difficult to parametrize correctly. Briefly, our analysis reveals that if  $\lambda$  is parametrized as  $\nu \exp(i\theta)$ , parametrization of  $\theta$  must depend on the one of  $\nu$ , but the reverse is not necessary. However, doing so does not hurt learning, as we exemplify in Appendix A.3.2.

#### 3.2 Several RNN architectures implicitly alleviates the curse of memory

State-space models, as well as gated RNNs, feature some form of normalization and reparametrization which facilitates signal propagation. We discuss how below.

**State-space models.** SSMs are originally motivated as discretizations of the continuous-time differential equation  $\dot{h} = Ah + Bx$  [16]. Naïve discretization of the differential equation yields  $h_{t+1} = (\text{Id} + dtA)h_t + dtBx_{t+1}$  which already acts as some input normalization when  $d_t$  is small.

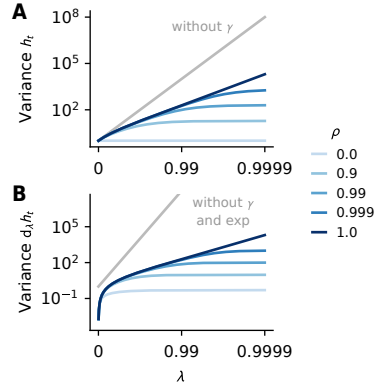


Figure 2: **Illustration of the effects of normalization and reparametrization.** It can effectively control the magnitude of **A.**  $\mathbb{E}[h_t^2]$  and **B.**  $\mathbb{E}[(d_\lambda h_t)^2]$  over all  $\lambda$  values when the input auto-correlation satisfies  $R_x(\Delta) = \rho^{|\Delta|}$  with  $\rho = 0$ , but does not manage to do so for other type of distributions ( $\rho \neq 0$ ). Here, we use  $\gamma(\lambda) = \sqrt{1 - \lambda^2}$ , decouple it from  $\lambda$  when differentiating, and take  $\lambda = \exp(-\exp(\nu))$  as in [20]. The grey line indicates the value the two quantities take without any normalization and reparametrization, when  $\rho = 1$ .

More elaborate discretization schemes, such as the zero-order hold, effectively reparametrize the  $A$  matrix, e.g. with  $\exp(dtA)$ . Here, diagonalization arises from computational efficiency and simplicity reasons [18]. While such models can approximate any smooth mappings [47, 48], their expressivity remains limited [49]. The next generation of these models, including Mamba [21], incorporates input-dependent gates which modulate  $dt$  depending on the input  $x_t$ . The theory we developed above does not strictly apply to this setting as  $dt$  is not constant. However, since the rest of the model’s structure remains unchanged we expect this behavior, and thus its remedies, to remain.

**Gated RNNs.** While the original motivation behind gated RNNs such as LSTMs [3] or GRUs [23] largely differs from the one of SSMs, they share similar mechanisms. In these networks, the memory content stored in hidden neurons can be erased through a forget gate, and incoming inputs can selectively be written in memory through an input gate. Mathematically, this corresponds to hidden state updates of the form  $h_{t+1} = f_{t+1} \odot h_t + i_{t+1} \odot x_{t+1}$ , with the forget  $f_{t+1}$  and input  $i_{t+1}$  gates being independent non-linear functions of  $x_{t+1}$  and  $h_t$ . The forget gate is akin to  $\lambda$  and usually involves a sigmoid non-linearity, which has a similar effect in the backward pass as reparametrizing  $\lambda$ . The input gate can act as an input normalization depending on the initialization of the network or if is coupled to the forget gate as in the GRU ( $f_t = 1 - i_t$ ) [29]. Importantly, the gates here depend on the hidden states and thus make the Jacobian  $\partial_{h_t} h_{t+1}$  non diagonal. Yet, we argue that these architectures still have a bias towards diagonality. Indeed, the contributions of the hidden state through the forget and input gates are indirect, and they can be ignored when the weights connecting the hidden states to the gates are small. We therefore get back to the setting we discussed in the previous paragraph; we confirm this intuition in Section 5. In regimes in which this approximation does not hold, studying signal propagation requires a much more sophisticated analysis than the one we have done here [50].

## 4 A linear teacher-student analysis

We consider a teacher-student task with linear recurrent networks [51]. This is arguably the simplest setting in which one can train recurrent networks, and yet, as we shall see, it is remarkably complex. We first turn to the one-dimensional setting to provide an intuitive illustration of how the curse of memory and vanishing gradients interplay. We then address the general setting and observe that linear networks indeed suffer from the curse of memory, and that the remedies we studied in the last section are effective. We additionally find that diagonality greatly modifies the structure of the loss landscape and helps optimizers with adaptive learning rates to compensate for an eventual increased sensitivity.

### 4.1 The one-dimensional case

We first consider a student and teacher following the one-dimensional dynamics  $h_{t+1} = \lambda h_t + x_{t+1}$ , with complex-valued parameter  $\lambda$  for the student and  $\lambda^*$  for the teacher. For simplicity, we draw  $x_{t+1}$  from a normal distribution with mean 0 and standard deviation 1 and note that other input distributions do not qualitatively change the results. The performance of the student is measured by a loss  $L$  that averages the per time-step losses  $L_t := \frac{1}{2}|h_t - h_t^*|^2$  over the entire sequence.

This simple model already captures two key difficulties of gradient-based learning of recurrent neural networks. In Figure 1, we plot the resulting loss landscape for different  $\lambda^*$  values, when  $\lambda$  evolves on the positive part of the real axis (Fig. 1.B) and when it evolves on the circle of radius  $|\lambda^*|$  in the complex plane (Fig. 1.C). We restrict  $\lambda$ s to have absolute values smaller than one: exploding gradients are out of the picture. Still, two difficulties for gradient-based learning appear here. On one side, vanishing gradients lead to flat loss regions that are hard to escape. On the other side, the loss sharpens as the student encodes longer memories because of the curse of memory. As a consequence, gradient-based optimization is extremely tedious, already in this simple example.

### 4.2 Diagonal connectivity simplifies optimization

We now move to the general case in which the teacher evolves according to

$$h_{t+1} = Ah_t + Bx_{t+1} \quad \text{and} \quad y_t = Ch_t + Dx_t. \quad (10)$$

with  $h_t \in \mathbb{R}^n$ ,  $x_t \in \mathbb{R}$  drawn i.i.d. from  $\mathcal{N}(0, 1)$ ,  $A \in \mathbb{R}^{n \times n}$ ,  $B \in \mathbb{R}^{n \times 1}$ ,  $C \in \mathbb{R}^{1 \times n}$  and  $D \in \mathbb{R}^{1 \times 1}$ . Here both inputs and outputs are scalars.

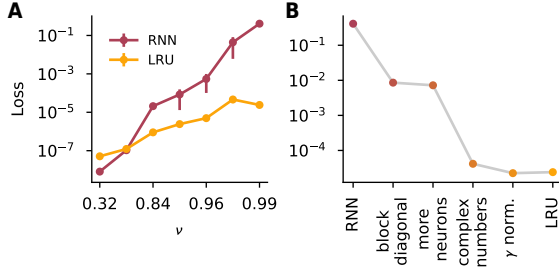


Figure 3: **LRUs are better at replicating a teacher’s behavior than linear RNNs.** **A.** As the teacher encodes longer dependencies ( $\nu \rightarrow 1$ ), the linear RNN struggles to reproduce it, but not the LRU. **B.** An ablation study ( $\nu = 0.99$ ) reveals that this gap mainly comes from having a  $2 \times 2$  block diagonal weight matrix, and then replacing those blocks with complex numbers.

Given the intuition we have developed so far, we expect fully connected linear recurrent neural networks to struggle in solving the task when the teacher encodes longer memories, not only because of exploding gradients but also due to the curse of memory. Conversely, diagonality facilitates eigenvalue reparametrization to avoid exploding gradients and make them better behaved. We run the following experiment to verify this intuition. We draw random teachers with hidden dimension  $n = 10$  and transform the complex eigenvalues of the recurrent matrix  $A$  to have magnitudes close to a value  $\nu$  that we control<sup>1</sup>. The larger  $\nu$  is, the longer the memories encoded by the teacher are. We train a linear RNN, as well as an LRU [20], with hidden dimension 64 on this task. The students are therefore largely overparametrized. We chose the LRU architecture to represent SSMs due to its simplicity. This architecture uses input normalization and an exponential reparametrization of the eigenvalues, similar to what we analyze in Section 3. Both networks are trained using the Adam optimizer [52] and cosine annealing schedule for 10k steps, on batches of size 128. The sequences contain 300 time steps. Learning rates are tuned separately for each method and training distribution. The results, which we plot in Figure 3.A, confirm our intuition: LRUs significantly outperform linear RNNs when long memories have to be learned, despite having 10 times fewer parameters.

Next, we wonder which design choices behind the LRU architecture are crucial to this performance improvement. To this end, we interpolate between a linear RNN and an LRU in the following way: First, we restrict the weight matrix of the linear RNN to a block diagonal with blocks of size 2. Each of such blocks can represent a complex number, so 32 complex numbers in total. We additionally double the number of hidden neurons. Second, we change those  $2 \times 2$  blocks (and their input and output weights) to be complex numbers. Finally, we add the  $\gamma$  input normalization and the exponential parametrization to obtain the final LRU architecture. We report the results of this experiment in Figure 3.B. We find that most of the gap comes from the introduction of complex numbers and can be partially reduced by making the weight matrix block diagonal. Interestingly, those two changes reduce the number of parameters the model has and slightly reduce the model expressivity so an explanation of this behavior is likely to be related to the optimization properties of those models. We confirm this hypothesis in the next section.

### 4.3 On the importance of adaptive learning rates

So far, our results highlight the importance of directly parametrizing the complex eigenvalues of the recurrent connectivity matrix. This parametrization does not mitigate any exploding behavior but modifies the loss landscape, making it possible for optimizers with adaptive learning rates to compensate for these behaviors. To demonstrate this, we study the Hessian of the loss:

$$\frac{d^2 L}{d\theta^2} = \sum_t \mathbb{E}_x \left[ \frac{dh_t}{d\theta} \frac{\partial^2 L_t}{\partial h_t^2} \frac{dh_t}{d\theta}^\top + \frac{\partial L_t}{\partial h_t} \frac{d^2 h_t}{d\theta^2} \right]. \quad (11)$$

If the network can perfectly fit the target data, which is the case here, the second term vanishes at optimality. We plot the Hessian at optimality in Figure 4.A and B for a standard linear recurrent network and one with complex diagonal parametrization, both with 4 hidden neurons ( $\nu = 0.99$ ). We observe that the eigenvalue spectra are similar for the two architectures, both exhibiting large terms that characteristic of the curse of memory, which makes learning with stochastic gradient

<sup>1</sup>We draw each entry of  $A$  from  $\mathcal{N}(0, 1/\sqrt{n})$ , complex diagonalize it, and apply the transformation  $x \mapsto \nu + (1 - \nu)\tanh(x)$  to the absolute values of the eigenvalues.

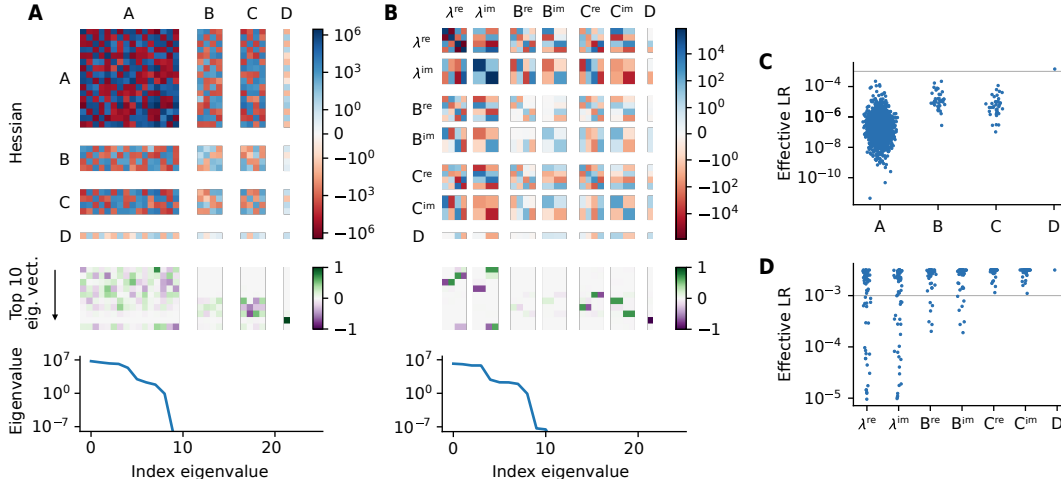


Figure 4: **Differences in learning abilities between fully connected and complex diagonal linear RNNs are due to a better structure of the loss landscape.** **A, B.** Hessian of the loss at optimality, its 10 eigenvectors with greatest eigenvalues and its eigenspectra for a fully connected RNN (A) and a complex diagonal one (B). The spectra are almost the same but top eigenvectors are concentrated on few coordinates for the complex diagonal one but not for the fully connected one. **C, D.** This structure makes it possible for Adam to efficiently deal with the extra sensitivity, as shown with the effective learning rates that it uses at the end of learning. For the fully connected one (C), Adam uses very low learning rates to compensate for the sensitivity, whereas it can use larger ones for the complex diagonal one without hindering training stability. The horizontal grey line shows the learning rate used, which is here  $10^{-3}$ .

descent almost impossible<sup>2</sup>. However, their structure differs. For the fully connected linear RNN, the top eigenvectors are distributed over many coordinates, whereas they are concentrated on a few coordinates for the complex diagonal one. This feature aids adaptive optimization [e.g., 56]: adapting to large curvature is much easier for Adam when the pathological directions are aligned to the canonical basis. This is what we observe in practice. In Figure 4.C and D, we compare the effective learning rate used by Adam, which we compute by providing a vector of ones to the optimizer. For the dense linear RNN, the adaptive learning rates cannot compensate for the intricate coupling between components, resulting in very small learning rates. Conversely, the sensitivity of complex diagonal RNNs is concentrated on few parameters, which adaptive learning rates can compensate for, leading to targeted and overall larger learning rates, significantly speeding up learning. As a side note, the complex eigenvalues of the teacher come in conjugate pairs. However, during training, the complex values of the complex RNN are not conjugates of each other, thereby increasing Hessian diagonality. Finally, performing this analysis for the LRU, we find that the Hessian spectrum is similar to the diagonal setting and that the exploding dimensions of the Hessian are almost exclusively due to the angle parameter, consistently with our theoretical analysis; see Figure 9.

Before concluding this section, we investigate whether there exist eigenvalue distributions that break the diagonal structure of the Hessian, making optimization harder and increasing the pressure on eigenvalue reparametrization. We theoretically prove in Appendix B.2 the intuitive result that the more concentrated the eigenvalues are, the less diagonal the Hessian is. As a consequence, the gap between complex-valued diagonal networks and LRUs widens, but the former still greatly outperform their fully-connected counterpart; see Figure 10.

<sup>2</sup>The gradient Lipschitz constant  $L$  of the loss equals the maximum Hessian eigenvalue [53]. This quantity sets a bound  $2/L$  for the maximum globally stable learning rate. While convergence might happen in a subspace, it is generally aligned with the top Hessian eigenspace near the solution [54, 55].



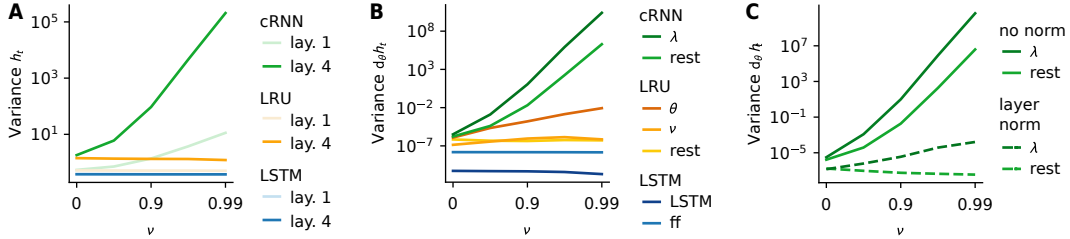


Figure 5: **Signal propagation in deep recurrent networks at initialization is consistent with our theory.** **A.**  $\mathbb{E}[h_t^2]$  after the first and the fourth layer, as a function of the memory parameter  $\nu$ , for complex-valued diagonal RNN (cRNN), LRU, and LSTM recurrent layers. The input normalization present in the LRU effectively keeps neural activity bounded. **B.** Comparison of the evolution of  $\mathbb{E}[d_\theta h_t^2]$  for the different recurrent layers and specific groups of parameters. For the complex diagonal RNN, the gradients of all parameters explode, whereas only the ones of  $\theta$  explode for the LRU. Regarding the LSTM, the magnitude of the gradients does not depend on  $\nu$ , with the LSTM-specific parameters exhibiting smaller gradients than the feedforward (ff) ones. **C.** Layer normalization keeps the overall gradient magnitude under control. Batch normalization yields similar results.

## 5 Signal propagation in deep recurrent networks at initialization

The ultimate goal of our theoretical quest is to gain practical insights into the training of recurrent networks. Specifically, we aim to verify whether the trends established theoretically and in controlled experiments hold in practice, by studying signal propagation at initialization.

We provide sequences of 512 text tokens as input to deep recurrent networks that contain four blocks of 256 hidden neurons each and use a next-token prediction loss to measure their performance. Each block consists of a recurrent layer followed by a feedforward gated linear unit [57]. By default, there are no normalization layers in this architecture. More details can be found in Appendix C.1. We empirically study how  $\mathbb{E}[h_t^2]$  and  $\mathbb{E}[d_\theta h_t^2]$  evolve when the memory of the recurrent layer, controlled by  $\nu$ , increases. We compare three different recurrent layers: a complex-valued diagonal RNN (cRNN), a LRU and a LSTM initialized with the chrono initialization [29].

The results are consistent with our theory. Complex-valued RNNs suffer from the curse of memory. LRUs almost perfectly mitigate this effect in the forward pass (Fig. 5.A) as well as in the backward pass (Fig. 5.B), except for the angle parameter  $\theta$ , as expected. We also wonder whether layer normalization can replace the input normalization and reparametrization of the LRU. We find that it mitigates the memory-induced gradient explosion at the macroscopic level (Fig. 5.C), but it likely kills any learning signal for the smallest eigenvalues. Finally, the LSTM manages to keep the gradient norm constant over different level of memory, consistently with the intuition we developed in Section 3.2, although the LSTM-specific parameters exhibit smaller gradients than the feedforward parameters.

## 6 Conclusion

Vanishing and exploding gradients complicate learning recurrent networks, but solving these problems is not enough. We uncovered yet another difficulty of training such networks, which is rooted in their iterative nature and arises at the edge of dynamical stability. Reparametrizations and adaptive learning rates can effectively mitigate this behavior in practice, and diagonalizing the recurrence simplifies both. Our analysis additionally reveals the complexity of learning the angle of complex eigenvalues, which may explain why complex numbers were not found to be useful in most recent state-space model architectures [21, 22].

A side finding of our study is the symbiosis between independent modules, which are here neurons and can more be more generally small heads, with adaptive learning rate optimizers in linear recurrent networks. Such a design pattern has promising properties: it facilitates online learning [58] and compositional generalization [59], allows for high level of parallelization [22], and matches, at a high level, the modular organization of the cortex in cortical columns [60]. Understanding how to increase the expressivity of small linear modules while keeping their great optimization properties constitutes a promising avenue for future research.

## **Acknowledgments**

The authors thank Robert Meier, João Sacramento, Guillaume Lajoie, Ezekiel Williams, Razvan Pascanu, Imanol Schlag and Bobby He for insightful discussions. Nicolas Zucchet was supported by an ETH Research Grant (ETH-23 21-1) and Antonio Orvieto acknowledges the financial support of the Hector Foundation.

## References

- [1] David E Rumelhart, Paul Smolensky, James L McClelland, and G Hinton. Sequential thought processes in PDP models. *Parallel distributed processing: explorations in the microstructures of cognition*, 2, 1986.
- [2] Jeffrey L Elman. Finding structure in time. *Cognitive science*, 14(2), 1990.
- [3] Sepp Hochreiter and Jürgen Schmidhuber. Long Short-Term Memory. *Neural Computation*, 9(8), 1997.
- [4] Ilya Sutskever, Oriol Vinyals, and Quoc V. Le. Sequence to sequence learning with neural networks. In *Advances in Neural Information Processing Systems*, 2014.
- [5] Sepp Hochreiter. *Untersuchungen zu dynamischen neuronalen Netzen*. Diploma thesis, Technische Universität München, 1991.
- [6] Yoshua Bengio, Patrice Simard, and Paolo Frasconi. Learning long-term dependencies with gradient descent is difficult. *IEEE transactions on neural networks*, 5(2), 1994.
- [7] Sepp Hochreiter, Yoshua Bengio, Paolo Frasconi, and Jürgen Schmidhuber. Gradient flow in recurrent nets: the difficulty of learning long-term dependencies. In *A field guide to dynamical recurrent networks*. IEEE, 2001.
- [8] Razvan Pascanu, Tomas Mikolov, and Yoshua Bengio. On the difficulty of training recurrent neural networks. In *International Conference on Machine Learning*, 2013.
- [9] Dzmitry Bahdanau, Kyunghyun Cho, and Yoshua Bengio. Neural machine translation by jointly learning to align and translate. In *International Conference on Learning Representations*, 2015.
- [10] Ashish Vaswani, Noam Shazeer, Niki Parmar, Jakob Uszkoreit, Llion Jones, Aidan N. Gomez, Łukasz Kaiser, and Illia Polosukhin. Attention is all you need. In *Advances in Neural Information Processing Systems*, 2017.
- [11] Quentin Fournier, Gaétan Marceau Caron, and Daniel Aloise. A practical survey on faster and lighter transformers. *ACM Computing Surveys*, 55(14s), 2023.
- [12] Angelos Katharopoulos, Apoorv Vyas, Nikolaos Pappas, and François Fleuret. Transformers are RNNs: fast autoregressive Transformers with linear attention. In *International Conference on Machine Learning*, 2020.
- [13] Tri Dao, Daniel Y. Fu, Stefano Ermon, Atri Rudra, and Christopher Ré. FlashAttention: fast and memory-efficient exact attention with IO-awareness. *arXiv preprint arXiv:2205.14135*, 2022.
- [14] William Fedus, Barret Zoph, and Noam Shazeer. Switch Transformers: scaling to trillion parameter models with simple and efficient sparsity. *Journal of Machine Learning Research*, 2022.
- [15] Shuming Ma, Hongyu Wang, Lingxiao Ma, Lei Wang, Wenhui Wang, Shaohan Huang, Li Dong, Ruiping Wang, Jilong Xue, and Furu Wei. The era of 1-bit LLMs: all Large Language Models are in 1.58 bits. *arXiv preprint arXiv:2402.17764*, 2024.
- [16] Albert Gu, Isys Johnson, Karan Goel, Khaled Saab, Tri Dao, Atri Rudra, and Christopher Ré. Combining recurrent, convolutional, and continuous-time models with linear state-space layers. In *Advances in Neural Information Processing Systems*, 2021.
- [17] Albert Gu, Karan Goel, and Christopher Ré. Efficiently modeling long sequences with structured state spaces. In *International Conference on Learning Representations*, 2022.
- [18] Ankit Gupta, Albert Gu, and Jonathan Berant. Diagonal state spaces are as effective as structured states spaces. In *Advances in Neural Information Processing Systems*, volume 35, 2022.
- [19] Jimmy T.H. Smith, Andrew Warrington, and Scott W. Linderman. Simplified state space layers for sequence modeling. In *International Conference on Learning Representations*, 2023.
- [20] Antonio Orvieto, Samuel L Smith, Albert Gu, Anushan Fernando, Caglar Gulcehre, Razvan Pascanu, and Soham De. Resurrecting recurrent neural networks for long sequences. In *International Conference on Machine Learning*, 2023.
- [21] Albert Gu and Tri Dao. Mamba: linear-time sequence modeling with selective state spaces. *arXiv preprint arXiv:2312.00752*, 2023.

- [22] Soham De, Samuel L. Smith, Anushan Fernando, Aleksandar Botev, George Cristian-Muraru, Albert Gu, Ruba Haroun, Leonard Berrada, Yutian Chen, Srivatsan Srinivasan, Guillaume Desjardins, Arnaud Doucet, David Budden, Yee Whye Teh, Razvan Pascanu, Nando De Freitas, and Caglar Gulcehre. Griffin: mixing gated linear recurrences with local attention for efficient language models. *arXiv preprint arXiv:2402.19427*, 2024.
- [23] Kyunghyun Cho, Bart van Merriënboer, Dzmitry Bahdanau, and Yoshua Bengio. On the properties of neural machine translation: encoder-decoder approaches. In *Proceedings of SSST-8, Eighth Workshop on Syntax, Semantics and Structure in Statistical Translation*, 2014.
- [24] Tomas Mikolov. *Statistical language models based on neural networks*. PhD thesis, Brno University of Technology, 2012.
- [25] Sergey Ioffe and Christian Szegedy. Batch normalization: accelerating deep network training by reducing internal covariate shift. In *International Conference on Machine Learning*, 2015.
- [26] Jimmy Lei Ba, Jamie Ryan Kiros, and Geoffrey E. Hinton. Layer normalization. In *Neural Information Processing Systems - Deep Learning Symposium*, 2016.
- [27] Tim Cooijmans, Nicolas Ballas, César Laurent, Çağlar Gülçehre, and Aaron Courville. Recurrent batch normalization. In *International Conference on Learning Representations*, 2017.
- [28] Quoc V. Le, Navdeep Jaitly, and Geoffrey E. Hinton. A simple way to initialize recurrent networks of rectified linear units. *arXiv preprint arXiv:1504.00941*, 2015.
- [29] Corentin Tallec and Yann Ollivier. Can recurrent neural networks warp time? In *International Conference on Learning Representations*, 2018.
- [30] Salah El Hahi and Yoshua Bengio. Hierarchical recurrent neural networks for long-term dependencies. In *Neural Information Processing Systems*, 1995.
- [31] Asier Mujika, Florian Meier, and Angelika Steger. Fast-slow recurrent neural networks. In *Neural Information Processing Systems*, 2017.
- [32] Martin Arjovsky, Amar Shah, and Yoshua Bengio. Unitary evolution recurrent neural networks. In *International Conference on Machine Learning*, 2016.
- [33] Eugene Vorontsov, Chiheb Trabelsi, Samuel Kadoury, and Chris Pal. On orthogonality and learning recurrent networks with long term dependencies. In *International Conference on Machine Learning*, 2017.
- [34] Kyle Helfrich, Devin Willmott, and Qiang Ye. Orthogonal recurrent neural networks with scaled Cayley transform. In *International Conference on Machine Learning*, 2018.
- [35] T. Konstantin Rusch and Siddhartha Mishra. Coupled oscillatory recurrent neural network (coRNN): an accurate and (gradient) stable architecture for learning long time dependencies. In *International Conference on Learning Representations*, 2021.
- [36] T Anderson Keller and Max Welling. Neural wave machines: learning spatiotemporally structured representations with locally coupled oscillatory recurrent neural networks. In *International Conference on Machine Learning*, 2023.
- [37] Il Memming Park, Ábel Ságodi, and Piotr Aleksander Sokół. Persistent learning signals and working memory without continuous attractors. *arXiv preprint arXiv:2308.12585*, 2023.
- [38] Zhong Li, Jiequn Han, Weinan E, and Qianxiao Li. Approximation and optimization theory for linear continuous-time recurrent neural networks. *Journal of Machine Learning Research*, 23(42), 2022.
- [39] Shida Wang, Zhong Li, and Qianxiao Li. Inverse approximation theory for nonlinear recurrent neural networks. In *International Conference on Learning Representations*, 2024.
- [40] James Martens and Ilya Sutskever. Learning recurrent neural networks with hessian-free optimization. In *International Conference on Machine Learning*, 2011.
- [41] Lorenzo Noci, Alexandru Meterez, Thomas Hofmann, and Antonio Orvieto. Why do learning rates transfer? Reconciling optimization and scaling limits for deep learning. *arXiv preprint arXiv:2402.17457*, 2024.
- [42] Greg Yang and Edward J Hu. Feature learning in infinite-width neural networks. *arXiv preprint arXiv:2011.14522*, 2020.

- [43] Greg Yang, James B Simon, and Jeremy Bernstein. A spectral condition for feature learning. *arXiv preprint arXiv:2310.17813*, 2023.
- [44] Xavier Glorot and Yoshua Bengio. Understanding the difficulty of training deep feedforward neural networks. In *Artificial Intelligence and Statistics*, 2010.
- [45] Kaiming He, Xiangyu Zhang, Shaoqing Ren, and Jian Sun. Delving Deep into Rectifiers: Surpassing Human-Level Performance on ImageNet Classification. In *International Conference on Computer Vision*, 2015.
- [46] Greg Yang, Edward J. Hu, Igor Babuschkin, Szymon Sidor, Xiaodong Liu, David Farhi, Nick Ryder, Jakub Pachocki, Weizhu Chen, and Jianfeng Gao. Tensor Programs V: Tuning Large Neural Networks via Zero-Shot Hyperparameter Transfer. *arXiv preprint arXiv:2203.03466*, 2022.
- [47] S. Boyd and L. Chua. Fading memory and the problem of approximating nonlinear operators with Volterra series. *IEEE Transactions on Circuits and Systems*, 32(11), 1985.
- [48] Antonio Orvieto, Soham De, Caglar Gulcehre, Razvan Pascanu, and Samuel L. Smith. Universality of linear recurrences followed by non-linear projections: finite-width guarantees and benefits of complex eigenvalues. In *International Conference on Machine Learning*, 2024.
- [49] William Merrill, Jackson Petty, and Ashish Sabharwal. The illusion of state in state-space models. In *International Conference on Machine Learning*, 2024.
- [50] Minmin Chen, Jeffrey Pennington, and Samuel S. Schoenholz. Dynamical isometry and a mean field theory of RNNs: gating enables signal propagation in recurrent neural networks. 2018.
- [51] Moritz Hardt, Tengyu Ma, and Benjamin Recht. Gradient descent learns linear dynamical systems. *Journal of Machine Learning Research*, 19(29), 2018.
- [52] Diederik P. Kingma and Jimmy Ba. Adam: a method for stochastic optimization. In *International Conference on Learning Representations*, 2015.
- [53] Yurii Nesterov and others. *Lectures on convex optimization*, volume 137. Springer, 2018.
- [54] Jeremy Cohen, Simran Kaur, Yuanzhi Li, J Zico Kolter, and Ameet Talwalkar. Gradient descent on neural networks typically occurs at the edge of stability. In *International Conference on Learning Representations*, 2020.
- [55] Guy Gur-Ari, Daniel A Roberts, and Ethan Dyer. Gradient descent happens in a tiny subspace. *arXiv preprint arXiv:1812.04754*, 2018.
- [56] Yan Pan and Yuanzhi Li. Toward understanding why Adam converges faster than SGD for transformers. *arXiv preprint arXiv:2306.00204*, 2023.
- [57] Yann N. Dauphin, Angela Fan, Michael Auli, and David Grangier. Language modeling with gated convolutional networks. In *International Conference on Machine Learning*, 2017.
- [58] Nicolas Zucchet, Robert Meier, Simon Schug, Asier Mujika, and João Sacramento. Online learning of long-range dependencies. In *Advances in Neural Information Processing Systems*, 2023.
- [59] Anirudh Goyal, Alex Lamb, Jordan Hoffmann, Shagun Sodhani, Sergey Levine, Yoshua Bengio, and Bernhard Schölkopf. Recurrent independent mechanisms. In *International Conference on Learning Representations*, 2021.
- [60] V B Mountcastle. The columnar organization of the neocortex. *Brain*, 120(4), 1997.
- [61] Christoph Boeddeker, Patrick Hanebrink, Lukas Drude, Jahn Heymann, and Reinhold Haeb-Umbach. On the computation of complex-valued gradients with application to statistically optimum beamforming. *arXiv preprint arXiv:1701.00392*, 2017.
- [62] James Bradbury, Roy Frostig, Peter Hawkins, Matthew James Johnson, Chris Leary, Dougal Maclaurin, George Necula, Adam Paszke, Jake VanderPlas, Skye Wanderman-Milne, and Qiao Zhang. JAX: composable transformations of Python+NumPy programs, 2018. URL <http://github.com/google/jax>.
- [63] Jonathan Heek, Anselm Levskaya, Avital Oliver, Marvin Ritter, Bertrand Rondepierre, Andreas Steiner, and Marc van Zee. Flax: A neural network library and ecosystem for JAX, 2023. URL <http://github.com/google/flax>.

- [64] Nicolas Zucchet, Robert Meier, and Simon Schug. Minimal LRU, 2023. URL <https://github.com/NicolasZucchet/minimal-LRU>.
- [65] Wikimedia Foundation. Wikimedia Downloads. URL <https://dumps.wikimedia.org>.
- [66] Jacob Devlin, Ming-Wei Chang, Kenton Lee, and Kristina Toutanova. BERT: Pre-training of Deep Bidirectional Transformers for Language Understanding. In Jill Burstein, Christy Doran, and Thamar Solorio, editors, *Proceedings of the 2019 Conference of the North American Chapter of the Association for Computational Linguistics: Human Language Technologies, Volume 1 (Long and Short Papers)*, 2019.

# Appendix

## Table of contents

---

<b>A Theory</b>	<b>16</b>
A.1 Useful lemmas . . . . .	16
A.2 The curse of memory: signal propagation analysis . . . . .	16
A.2.1 Forward pass . . . . .	17
A.2.2 Backward pass . . . . .	17
A.2.3 Extension to fully-connected networks . . . . .	19
A.3 Impact of input normalization and parametrization . . . . .	20
A.3.1 Real case . . . . .	20
A.3.2 On the difficulty of parametrizing complex numbers . . . . .	20
<b>B Linear teacher-student task</b>	<b>21</b>
B.1 1D setting . . . . .	21
B.1.1 Calculation of the loss . . . . .	21
B.1.2 Optimal normalization and reparametrization with uncorrelated inputs . .	22
B.1.3 Visualization of the effect of input normalization and reparametrization .	23
B.1.4 Learning the angle is difficult in practice: an example . . . . .	24
B.2 Structure of the Hessian at optimality . . . . .	25
B.2.1 Hessian for complex-valued variables . . . . .	25
B.2.2 Hessian with respect to the recurrent eigenvalues . . . . .	26
B.2.3 Hessian for different parametrizations . . . . .	28
B.3 Experimental details . . . . .	29
B.4 Additional analyses . . . . .	31
B.4.1 Structure of the loss landscape for LRUs . . . . .	31
B.4.2 Concentrating eigenvalue distributions . . . . .	31
<b>C Signal propagation in deep recurrent neural networks at initialization</b>	<b>32</b>
C.1 Experimental setup . . . . .	32

---

## A Theory

This section introduces all the theoretical results we directly or indirectly mention in the main text, as well as provides a proof for them.

### A.1 Useful lemmas

Most, if not all the calculations, that we will be doing in this section involves infinite sums. We state and prove two useful lemmas to simplify later calculations.

**Lemma 1.** For  $\alpha, \beta \in \mathbb{C}$  satisfying  $|\alpha| < 1$  and  $|\beta| < 1$ , and  $(u_n)_{n \in \mathbb{Z}}$  a bounded sequence satisfying  $u_{-n} = u_n$ , we have

$$\sum_{n,m \geq 0} \alpha^n \beta^m u_{n-m} = \frac{1}{1 - \alpha\beta} \left( u_0 + \sum_{\Delta \geq 1} (\alpha^\Delta + \beta^\Delta) u_\Delta \right) \quad (12)$$

*Proof.* The proof naturally comes from separating the indices  $n$  and  $m$  in three sets: one in which the two are equals, one in which  $n$  is larger and one in which  $m$  is larger. This gives

$$\sum_{n,m \geq 0} \alpha^n \beta^m u_{n-m} = \sum_{n=m} \alpha^n \beta^m u_{n-m} + \sum_{n>m} \alpha^n \beta^m u_{n-m} + \sum_{n<m} \alpha^n \beta^m u_{n-m} \quad (13)$$

$$= \sum_n \alpha^n \beta^n u_0 + \sum_m \alpha^m \beta^m \sum_{\Delta \geq 1} \alpha^\Delta u_\Delta + \sum_n \alpha^n \beta^n \sum_{\Delta \geq 1} \beta^\Delta u_{-\Delta} \quad (14)$$

$$= \sum_n \alpha^n \beta^n \left( 1 + \sum_{\Delta \geq 1} (\alpha^\Delta + \beta^\Delta) u_\Delta \right) \quad (15)$$

$$= \frac{1}{1 - \alpha\beta} \left( 1 + \sum_{\Delta \geq 1} (\alpha^\Delta + \beta^\Delta) u_\Delta \right) \quad (16)$$

□

**Lemma 2.** In the same conditions as Lemma 1, we have

$$\sum_{n,m \geq 0} nm \alpha^{n-1} \beta^{m-1} u_{n-m} = \frac{d}{d\alpha} \frac{d}{d\beta} \left[ \frac{1}{1 - \alpha\beta} \left( u_0 + \sum_{\Delta \geq 1} (\alpha^\Delta + \beta^\Delta) u_\Delta \right) \right] \quad (17)$$

*Proof.* This follows from remarking that

$$\frac{d}{d\alpha} \frac{d}{d\beta} \left[ \sum_{n,m \geq 0} \alpha^n \beta^m u_{n-m} \right] = \frac{d}{d\alpha} \left[ \sum_{n,m \geq 0} m \alpha^n \beta^{m-1} u_{n-m} \right] \quad (18)$$

$$= \sum_{n,m \geq 0} nm \alpha^{n-1} \beta^{m-1} u_{n-m} \quad (19)$$

and using Lemma 1 to get the final result. □

### A.2 The curse of memory: signal propagation analysis

We recall the assumptions that we stated in Section 2.2:

- a) **Linear diagonal recurrent neural networks.** We restrict ourselves to networks satisfying  $h_{t+1} = \lambda \odot h_t + x_{t+1}$  with  $\lambda$ ,  $h_t$  and  $x_t$  complex numbers. Without loss of generality, we focus on the one dimensional setting. We additionally consider  $\lambda$ s with absolute values smaller than 1.
- b) **Infinite time horizon.** We consider infinite sequences and initialize the network dynamics at  $t_0 = -\infty$ .



- c) **Wide-sense stationarity.** We assume the different quantities that the network receives, which includes the inputs  $x_t$ , to be wide-sense stationary (WSS). A random process  $X_t$  is said to be WSS if its auto-correlation function is independent of time, that is, for all  $t \in \mathbb{R}$  and  $\Delta \in \mathbb{R}$ ,  $\mathbb{E}[X_{t+\Delta}\bar{X}_t] := R_X(\Delta)$ .

### A.2.1 Forward pass

Without loss of generality, we can take  $t = 0$  given the wide-sense stationarity and infinite time horizon assumptions. Let us first remark that we have

$$h_0 = \sum_{n \geq 0} \lambda^n x_{-n} \quad (20)$$

so that

$$\mathbb{E}[|h_0|^2] = \sum_{n,m \geq 0} \lambda^n \bar{\lambda}^m \mathbb{E}[x_{-n} \bar{x}_{-m}] \quad (21)$$

$$= \sum_{n,m \geq 0} \lambda^n \bar{\lambda}^m R_x(n-m) \quad (22)$$

$$= \frac{1}{1-|\lambda|^2} \left( R_x(0) + \sum_{\Delta \geq 1} (\bar{\lambda}^\Delta + \lambda^\Delta) R_x(\Delta) \right). \quad (23)$$

We used Lemma 1 to obtain the last equality. In Section 2.2, we focused on the real case  $\bar{\lambda} = \lambda$ , so this formula becomes Equation 5. If we further assume that the auto-correlation of  $x$  decreases exponentially with decay rate  $\rho$ , that is  $R_x(\Delta) = \rho^{|\Delta|}$ , we can further simplify the last expression:

$$\mathbb{E}[|h_0|^2] = \frac{1}{1-|\lambda|^2} \left( 1 + \sum_{\Delta \geq 1} (\bar{\lambda}^\Delta + \lambda^\Delta) \rho^\Delta \right) \quad (24)$$

$$= \frac{1}{1-|\lambda|^2} \left( 1 + \frac{\bar{\lambda}\rho}{1-\bar{\lambda}\rho} + \frac{\lambda\rho}{1-\lambda\rho} \right) \quad (25)$$

$$= \frac{1-\rho^2|\lambda|^2}{|1-\rho\lambda|^2(1-|\lambda|^2)} \quad (26)$$

It follows that if the inputs are i.i.d. ( $\rho = 0$ ), we have  $\mathbb{E}[|h_0|^2] = (1-|\lambda|^2)^{-1}$ , and if the inputs are constant equal to 1 ( $\rho = 1$ ), we have  $\mathbb{E}[|h_0|^2] = |1-\lambda|^{-2}$ .

### A.2.2 Backward pass

Differentiating the update  $h_{t+1} = \lambda h_t + x_{t+1}$  with respect to  $\lambda$  gives

$$\frac{dh_t}{d\lambda} = \lambda \frac{dh_{t-1}}{d\lambda} + h_{t-1} \quad (27)$$

so that

$$\frac{dh_0}{d\lambda} = \sum_{n \geq 0} \lambda^n h_{-n} \quad (28)$$

$$= \sum_{n \geq 0} \lambda^n \sum_{m \geq 0} \lambda^m x_{-n-m} \quad (29)$$

$$= \sum_{n,m \geq 0} \lambda^{n+m} x_{-(n+m)} \quad (30)$$

$$= \sum_{n \geq 0} n \lambda^{n-1} x_{-n}. \quad (31)$$

Note that some extra technicalities are needed to justify these equations as  $\lambda$  and  $h_t$  are complex valued: these formulas hold as they would in the real-valued case as  $h_t$  is an holomorphic function of  $\lambda$ .

We can now compute the variance of the sensitivity of the hidden state with respect to the parameters.

$$\mathbb{E} \left[ \left| \frac{dh_t}{d\lambda} \right|^2 \right] = \sum_{n \geq 0} \sum_{m \geq 0} nm \lambda^{n-1} \bar{\lambda}^{m-1} R_x(n-m). \quad (32)$$

Using Lemma 2 gives

$$\mathbb{E} \left[ \left| \frac{dh_t}{d\lambda} \right|^2 \right] = \frac{d}{d\alpha} \frac{d}{d\beta} \left[ \frac{1}{1-\alpha\beta} \left( R_x(0) + \sum_{\Delta \geq 1} (\alpha^\Delta + \beta^\Delta) R_x(\Delta) \right) \right]_{\alpha=\lambda, \beta=\bar{\lambda}}. \quad (33)$$

Differentiating this quantity as a product gives

$$\begin{aligned} \mathbb{E} \left[ \left| \frac{dh_t}{d\lambda} \right|^2 \right] &= \left[ \frac{1+\alpha\beta}{(1-\alpha\beta)^3} \left( R_x(0) + \sum_{\Delta \geq 1} (\alpha^\Delta + \beta^\Delta) R_x(\Delta) \right) + 0 \right. \\ &\quad \left. + \frac{\alpha}{(1-\alpha\beta)^2} \left( \sum_{\Delta \geq 1} \Delta \alpha^{\Delta-1} R_x(\Delta) \right) + \frac{\beta}{(1-\alpha\beta)^2} \left( \sum_{\Delta \geq 1} \Delta \beta^{\Delta-1} R_x(\Delta) \right) \right]_{\alpha=\lambda, \beta=\bar{\lambda}}, \quad (34) \end{aligned}$$

which then simplifies as

$$\begin{aligned} \mathbb{E} \left[ \left| \frac{dh_t}{d\lambda} \right|^2 \right] &= \frac{1+|\lambda|^2}{(1-|\lambda|)^3} \left( R_x(0) + \sum_{\Delta \geq 1} (\lambda^\Delta + \bar{\lambda}^\Delta) R_x(\Delta) \right) \\ &\quad + \frac{1}{(1-|\lambda|^2)^2} \left( \sum_{\Delta \geq 1} \Delta (\lambda^\Delta + \bar{\lambda}^\Delta) R_x(\Delta) \right). \quad (35) \end{aligned}$$

Note that Equation 6 in the main text is the real-valued version of that formula.

Let us now further simplify this equation when  $R_x(\Delta) = \rho^{|\Delta|}$ . If we use this in the differentiated quantity before differentiating it, we get

$$\mathbb{E} \left[ \left| \frac{dh_t}{d\lambda} \right|^2 \right] = \frac{d}{d\alpha} \frac{d}{d\beta} \left[ \frac{1}{1-\alpha\beta} \left( \frac{1-\rho^2\alpha\beta}{(1-\rho\alpha)(1-\rho\beta)} \right) \right]_{\alpha=\lambda, \beta=\bar{\lambda}}. \quad (36)$$

Calculating this quantity manually is painful. Instead, we use the following trick. Its denominator is rather easy to compute, it is equal to  $(1-\alpha\beta)^3(1-\rho\alpha)^2(1-\rho\beta)^2$ . We thus multiply it to the derivative of the function we want to compute in order to obtain a polynomial with unknown factors, and use polynomial regression tools to derive the resulting coefficients. Massaging the obtained expression to make it easier to compute the closed-form value of this quantity when  $\rho = 0$  and  $\rho = 1$ , we get

$$\mathbb{E} \left[ \left| \frac{dh_t}{d\lambda} \right|^2 \right] = \frac{(1-\rho)(1+|\lambda|^2) + \rho^2(1-|\lambda|^2)^3 + \rho(1-\rho)|\lambda|^2(\rho|\lambda|^2(1+|\lambda|^2) - 2\lambda - 2\bar{\lambda})}{(1-|\lambda|^2)^3|1-\rho\lambda|^4}. \quad (37)$$

This is the quantity we plot on Figure 1.A, when  $\lambda$  is real-valued. When  $\rho = 0$ , this quantity becomes

$$\mathbb{E} \left[ \left| \frac{dh_t}{d\lambda} \right|^2 \right] = \frac{1+|\lambda|^2}{(1-|\lambda|^2)^3}, \quad (38)$$

and it is equal to

$$\mathbb{E} \left[ \left| \frac{dh_t}{d\lambda} \right|^2 \right] = \frac{1}{|1-\lambda|^4}, \quad (39)$$

when  $\rho = 1$ . Additionally, it will diverge whenever  $|\lambda| \rightarrow 1$  when  $\rho < 1$ , and when  $\lambda \rightarrow 1$  when  $\rho = 1$ .

Regarding the backpropagation of errors to the inputs, the analysis we did in the main text also holds for complex number given that  $h_t$  is an holomorphic function of  $x_t$  and it thus behaves as the forward pass once replacing the input distribution with the one of output errors  $\partial_{h_t} L_t$ .

### A.2.3 Extension to fully-connected networks

We now turn to the non-diagonal case. For the sake of simplicity, we assume that recurrent matrix is complex diagonalizable and that its eigenvalues are all different. This will enable us to differentiate the eigenvalues and the eigenvectors. We consider dynamics of the form

$$h_{t+1} = Ah_t + x_{t+1} \quad (40)$$

As  $A$  is complex diagonalizable, there exists a complex-valued matrix  $P$  and a complex-valued vector  $\lambda$  such that

$$A = P \text{diag}(\lambda) P^{-1} \quad (41)$$

$$P_{:i}^\dagger P_{:i} = 1 \quad \forall i. \quad (42)$$

The linear recurrent neural network considered above is equivalent to its diagonal version

$$h_{t+1}^{\text{diag}} = \lambda h_t^{\text{diag}} + P^{-1} x_{t+1} \quad (43)$$

$$h_t = P h_t^{\text{diag}}. \quad (44)$$

We now differentiate  $h_t$  w.r.t. to  $A$  using the diagonal parametrization and obtain

$$\frac{dh_t}{dA} = \frac{\partial h_t}{\partial P} \frac{\partial P}{\partial A} + \frac{\partial h_t}{\partial h_t^{\text{diag}}} \frac{dh_t^{\text{diag}}}{d\lambda} \frac{\partial \lambda}{\partial A} + \frac{\partial h_t}{\partial h_t^{\text{diag}}} \frac{dh_t^{\text{diag}}}{dP^{-1}} \frac{\partial P^{-1}}{\partial A}. \quad (45)$$

$d_A P$ ,  $d_A P^{-1}$  and  $d_A \lambda$  can be considered constant. Intuitively, the eigenvalues and eigenvectors move smoothly as we restricted ourselves to the case in which eigenvalues are singular. If this is not the case, math becomes trickier as the eigenvectors are not uniquely defined. We can study the behavior of those quantities in more detail, following Boeddeker et al. [61]:

$$\frac{\partial \lambda}{\partial A_{ij}} = \text{diag} \left( P^{-1} \frac{\partial A}{\partial A_{ij}} P \right) \quad (46)$$

$$\frac{dP}{dA_{ij}} = P \left( F \odot \left( P^{-1} \frac{\partial A}{\partial A_{ij}} P \right) \right) \quad (47)$$

The  $F$  introduced in the last equation is equal to

$$F_{ij} := \begin{cases} \frac{1}{\lambda_j - \lambda_i} & \text{if } i \neq j \\ 0 & \text{otherwise.} \end{cases} \quad (48)$$

Importantly, those two quantities do not grow to infinity as the absolute value of the eigenvalues goes to 1, which means that we can consider those derivatives to be independent of  $|\lambda|$  for the sake of our analysis. Note that the previous argument assumes that eigenvalues do not collapse.

$d_\lambda h_t^{\text{diag}}$  is the dominating term in  $d_A h_t$ . We wonder which of the three different terms that appear in  $d_A h_t$  (Equation 45) will be the dominating one as  $|\lambda|$  (or  $\lambda$ ) goes to 1. In the previous paragraph, we have shown that the derivative of  $P^{-1}$ ,  $P$  and  $\lambda$  can be considered constant for the sake of our analysis. We thus focus on the other terms.

First, we have

$$\frac{\partial h_{t,l}}{\partial P_{ij}} = h_{t,i}^{\text{diag}} \mathbb{1}_{j=l} \quad (49)$$

so the magnitude of this quantity is roughly the one of  $h_t^{\text{diag}}$ , which corresponds to the low pass filtering of the inputs with different  $\lambda$  values.

Second, we know that  $\partial_{h_t^{\text{diag}}} h_t$  does not change in magnitude as  $\lambda$  changes, as  $P$  remains bounded.

So, for the third term of the sum, we are left to study the behavior of  $d_{P^{-1}} h_t^{\text{diag}}$ . We can show that it evolves according to

$$\frac{dh_{t+1,k}^{\text{diag}}}{dP_{ij}^{-1}} = \lambda_i \frac{dh_{t+1,k}^{\text{diag}}}{dP_{ij}^{-1}} + x_{t+1,j} \quad \text{if } k = i \quad (50)$$

$$\frac{dh_{t+1,k}^{\text{diag}}}{dP_{ij}^{-1}} = 0 \quad \text{otherwise.} \quad (51)$$

It follows that the third term in the sum also corresponds to a low pass filtering of the inputs.

Finally, we know that the second term, the one in  $d_\lambda h_t^{\text{diag}}$  will grow faster to infinity as it corresponds to two consecutive low pass filters with the same  $\lambda$  values (c.f. calculation above). It will thus be the dominating term in the infinite memory limit.

### A.3 Impact of input normalization and parametrization

In this section, we consider a diagonal linear recurrent neural network of the form

$$h_{t+1} = \lambda(\omega)h_t + \gamma(\lambda)x_{t+1} \quad (52)$$

with  $\gamma(\lambda)$  the input normalization factor and  $\lambda$  parametrized by a vector  $\omega$ . Next, we study the effect of input normalization and reparametrization, first in the real-valued setting and then in the complex-valued one.

#### A.3.1 Real case

Let us start with the forward pass: as

$$h_t = \sum_{n \geq 0} \lambda^n \gamma(\lambda) x_{t-n}, \quad (53)$$

$\gamma$  rescales the value the hidden state takes. To avoid any explosion behavior, we thus ideally want  $\gamma$  to be the inverse of value of  $\mathbb{E}[(h_t)^2]$  without normalization, which we have computed in Equation 23. The same behavior holds for the backpropagation of errors to the inputs as

$$\frac{dL}{dx_t} = \gamma(\lambda) \left( \lambda \frac{dL}{dx_{t+1}} + \frac{\partial L}{\partial h_t} \right). \quad (54)$$

We now move to the impact of the parametrization. To simplify the calculation, we will ignore the dependency of  $\gamma$  on  $\lambda$  when differentiating it. This can easily be done in automatic differentiation software by removing this dependency from the computational graph with  $\gamma(\text{stop\_gradient}(\lambda))$ . We then have

$$\frac{dh_t}{d\omega} = \frac{dh_t}{d\lambda} \frac{d\lambda}{d\omega} \quad (55)$$

and  $d_\lambda h_t$  which is rescaled by  $\gamma$  compared to the calculation we did above. As a consequence, both the input normalization and the parametrization can help to mitigate the curse of memory.

#### A.3.2 On the difficulty of parametrizing complex numbers

We now extend the previous analysis to the complex case, and take a polar parametrization of  $\lambda$ :  $\lambda(\omega) = \nu(\omega) \exp(i\theta(\omega))$ . The effect of the input normalization does not change when moving to complex numbers. The role of the reparametrization is however a bit more subtle. As  $h_t$  is an holomorphic function of  $\lambda$ , we have  $d_{\bar{\lambda}} h_t = 0$  and

$$\frac{dh_t}{d\omega} = \frac{dh_t}{d\lambda} \frac{d\lambda}{d\omega} = \frac{dh_t}{d\lambda} \left( \frac{1}{2} \frac{d\nu}{d\omega} \exp(i\theta) + \frac{i}{2} \nu \frac{d\theta}{d\omega} \exp(i\theta) \right). \quad (56)$$

It follows that

$$\mathbb{E} \left[ \left| \frac{dh_t}{d\omega} \right|^2 \right] = \frac{1}{4} \mathbb{E} \left[ \left| \frac{dh_t}{d\lambda} \right|^2 \right] \left| \frac{d\nu}{d\omega} \exp(i\theta) + i\nu \frac{d\theta}{d\omega} \exp(i\theta) \right|^2 \quad (57)$$

$$= \frac{1}{4} \mathbb{E} \left[ \left| \frac{dh_t}{d\lambda} \right|^2 \right] \left| \frac{d\nu}{d\omega} + i\nu \frac{d\theta}{d\omega} \right|^2 \quad (58)$$

$$= \frac{1}{4} \mathbb{E} \left[ \left| \frac{dh_t}{d\lambda} \right|^2 \right] \left( \frac{d\nu}{d\omega}^2 + \nu^2 \frac{d\theta}{d\omega}^2 \right). \quad (59)$$

To simplify the analysis, we will further assume that  $\mathbb{E}[|d_\lambda h_t|^2]$  is only a function of  $\nu$ . This assumption holds in the case of  $\rho = 0$  and  $\rho = 1$ , c.f. Section A.2.2, but not necessarily otherwise. To ensure that

that this quantity does not depend on  $\lambda$ , we thus want  $d_\omega \nu^2 E(\nu) = \Theta(1)$  and  $\nu^2 d_\omega \theta^2 E(\nu) = \Theta(1)$ . The second means that the angle parametrization must depend on the value  $\nu$  takes. Let us take the  $\rho = 0$  example to get an idea of what the ideal parametrization should be. First, we have  $\gamma(\lambda) = \sqrt{1 - \nu^2}$  so that

$$E(\nu) = \gamma(\lambda)^2 \frac{1 + \nu^2}{(1 - \nu^2)^3} = \frac{1 + \nu^2}{(1 - \nu^2)^2}. \quad (60)$$

We are left with the differential equation  $\nu' = \Theta(1 - \nu^2)$ , which is for example solved with  $\nu = \tanh(\omega_\nu)$ . Now let us look at the parametrization of  $\theta$ . If we ignore the  $\nu^2$  term for simplicity, the approximate differential equation it needs to solve is  $d_\omega \theta = \Theta(1 - \nu^2)$ , which can be solved by  $\theta = \text{stop\_gradient}(1 - \nu^2)\omega_\theta$ . The exact detail of this calculation do not really matter as this is heavily input distribution dependent. However, the interesting part here is that the angle parameter must be rescaled by a function of  $\nu$ . This makes intuitive sense when looking looking at the sharpness of the loss around optimality in Figure 1.C, but this also makes the loss even flatter further away from optimality. We will come back to this point in Section B.1.4, showing that in practice, such a parametrization complicates the learning of the  $\theta$ . Learning complex numbers is thus difficult, because of the angle.

## B Linear teacher-student task

This section is dedicated to detail the theoretical results behind our analysis of the teacher-student task, present all the details necessary to reproduce our empirical experiments, and provide additional analysis.

### B.1 1D setting

#### B.1.1 Calculation of the loss

In this toy example, we are interested in learning a simple 1-dimensional linear recurrent neural network which follows the dynamics

$$h_{t+1} = \lambda h_t + x_{t+1} \quad (61)$$

to reproduce the hidden state  $h_t^*$  of a teacher with recurrent parameter  $\lambda^*$ . Note that we here allow all variables to be complex-valued. We take the loss to be

$$L(\lambda, \lambda^*) := \frac{1}{2T} \sum_{t=1}^T \mathbb{E}_x \left[ |h_t - h_t^*|^2 \right] \quad (62)$$

We assume  $x$  to be drawn from a wide-sense stationary distribution so that we can focus on studying the behavior of one  $L_t(\lambda, \lambda^*) := \frac{1}{2} \mathbb{E}_x \left[ |h_t - h_t^*|^2 \right]$  to understand the behavior of the full loss  $L$ , in the limit of infinitely long sequences ( $T \rightarrow \infty$ ). Moreover, to further simplify the calculations, we assume that  $x$  is real-valued and that  $R_x(\Delta) = \rho^{|\Delta|}$ .

Let us now proceed with the calculation:

$$L_t(\lambda, \lambda^*) := \frac{1}{2} \mathbb{E}_x \left[ h_t \bar{h}_t + h_t^* \bar{h}_t^* - h_t \bar{h}_t^* - \bar{h}_t h_t^* \right]. \quad (63)$$

We have shown in Section A.2 that in the limit of  $t \rightarrow \infty$ ,

$$\mathbb{E}_x \left[ h_t \bar{h}_t \right] = \frac{1}{1 - \lambda \bar{\lambda}} \left( 1 + \frac{\rho \lambda}{1 - \rho \lambda} + \frac{\rho \bar{\lambda}}{1 - \rho \bar{\lambda}} \right) \quad (64)$$

$$(65)$$

Similar derivations hold for the other three terms in the loss. Grouping them gives the exact value of the loss. We omit the formula as it is not particularly insightful. In the case of constant inputs ( $\rho = 1$ ), we have

$$L_t(\lambda, \lambda^*) = \frac{1}{2} \left| \frac{1}{1 - \lambda} - \frac{1}{1 - \lambda^*} \right|^2. \quad (66)$$

In the case of i.i.d. inputs ( $\rho = 0$ ), we have

$$L_t(\lambda, \lambda^*) = \frac{1}{2} \left( \frac{1}{1 - |\lambda|^2} + \frac{1}{1 - |\lambda^*|^2} - \operatorname{Re} \left[ \frac{2}{1 - \bar{\lambda}\lambda^*} \right] \right). \quad (67)$$

This is the loss we plot on Figure 1.B and C.

### B.1.2 Optimal normalization and reparametrization with uncorrelated inputs

Having a simple closed-form solution for the value the loss takes gives us the possibility to investigate in more detail what an optimal normalization and parametrization should be. We focus on the case  $\rho = 0$ .

For  $\rho = 0$ , the optimal normalization is  $\gamma(\lambda) = \sqrt{1 - |\lambda|^2}$ . Given that we now add an input normalization to the student, we must also add it to the teacher for the student to be able to fit it. The loss becomes

$$L_t = \frac{1}{2} \left( \frac{\gamma(\lambda)}{1 - |\lambda|^2} + \frac{\gamma(\lambda^*)}{1 - |\lambda^*|^2} - \operatorname{Re} \left[ \frac{2\gamma(\lambda)\gamma(\lambda^*)}{1 - \bar{\lambda}\lambda^*} \right] \right) \quad (68)$$

$$= 1 - \operatorname{Re} \left[ \frac{\gamma(\lambda)\gamma(\lambda^*)}{1 - \bar{\lambda}\lambda^*} \right]. \quad (69)$$

Next, we parametrize  $\lambda$  as  $\lambda = \nu(\omega_\nu) \exp(i\theta(\omega_\theta))$  and seek to find a parametrization such that, at optimality,  $\mathbb{E}[(d_{\omega_\nu} h_t)^2] = 1$  and  $\mathbb{E}[(d_{\omega_\theta} h_t)^2] = 1$ . Given that the student perfectly fit the teacher-generated data at optimality and that the loss we use is the mean-squared error, this corresponds to having  $d_{\omega_\nu}^2 L_t = 1$  and  $d_{\omega_\theta}^2 L_t = 1$ .

**Deriving the optimal  $\nu$  parametrization.** We now compute the Hessian of the loss w.r.t.  $\omega_\nu$ . First, we can simplify our calculations by restricting ourselves to the case  $\theta = \theta^*$ . The loss becomes

$$L_t = 1 - \frac{\gamma(\nu)\gamma(\nu^*)}{1 - \nu\nu^*}. \quad (70)$$

Differentiating this function a first time, we obtain

$$\frac{dL_t}{d\nu} = -\frac{\gamma(\nu^*)\gamma'(\nu)}{1 - \nu\nu^*} - \frac{\gamma(\nu^*)\nu^*\gamma(\nu)}{(1 - \nu\nu^*)^2}. \quad (71)$$

Differentiating it a second time gives

$$\frac{d^2 L_t}{d\nu^2} = -\frac{\gamma(\nu^*)\gamma''(\nu)}{1 - \nu\nu^*} - \frac{2\gamma(\nu^*)\nu^*\gamma'(\nu)}{(1 - \nu\nu^*)^2} - \frac{2\gamma(\nu^*)\nu^{*2}\gamma(\nu)}{(1 - \nu\nu^*)^3}. \quad (72)$$

Leveraging the fact that

$$\gamma'(\nu) = \frac{-\nu}{\gamma(\nu)} \quad \text{and} \quad \gamma''(\nu) = \frac{-\gamma(\nu)^2 - \nu^2}{\gamma(\nu)^3}, \quad (73)$$

we finally get, when  $\nu = \nu^*$ ,

$$\frac{d^2 L_t}{d\nu^2} = \frac{1}{(1 - \nu^2)^2}. \quad (74)$$

Given that we are at optimality, we have

$$\frac{d^2 L_t}{d\omega_\nu^2} = \mathbb{E} \left[ \frac{dh_t}{d\omega_\nu} \frac{d^2 L_t}{dh_t^2} \frac{dh_t}{d\omega_\nu} \right] = \nu'(\omega_\nu)^2 \mathbb{E} \left[ \frac{dh_t}{d\nu} \frac{d^2 L_t}{dh_t^2} \frac{dh_t}{d\nu} \right] = \nu'(\omega_\nu)^2 \frac{d^2 L_t}{d\nu^2}. \quad (75)$$

To keep that quantity constant, we thus have to solve the differential equation

$$\nu'(\omega_\nu) = (1 - \nu^2), \quad (76)$$

which gives  $\nu(\omega_\nu) = \tanh(\omega_\nu)$ .

**Deriving the optimal  $\theta$  parametrization.** We now move to the parametrization of  $\theta$ . We have

$$L_t = 1 - \operatorname{Re} \left[ \frac{\gamma(\nu)\gamma(\nu^*)}{1 - \bar{\lambda}\lambda^*} \right] = 1 - \frac{\gamma(\nu)\gamma(\nu^*)(1 - \nu\nu^* \cos(\theta - \theta^*))}{|1 - \bar{\lambda}\lambda^*|^2}. \quad (77)$$

For notational convenience, we denote

$$\alpha(\theta - \theta^*) := |1 - \bar{\lambda}\lambda^*|^2 = (1 - \nu\nu^* \cos(\theta - \theta^*))^2 + \nu^2\nu^{*2} \sin(\theta - \theta^*)^2. \quad (78)$$

We have

$$\frac{dL_t}{d\theta} = \gamma(\nu)\gamma(\nu^*) \left( -\frac{\nu\nu^* \sin(\theta - \theta^*)}{\alpha(\theta - \theta^*)} + \frac{(1 - \nu\nu^* \cos(\theta - \theta^*))\alpha'(\theta - \theta^*)}{\alpha(\theta - \theta^*)^2} \right) \quad (79)$$

and

$$\begin{aligned} \frac{d^2L_t}{d\theta^2} = \gamma(\nu)\gamma(\nu^*) & \left( -\frac{\nu\nu^* \cos(\theta - \theta^*)}{\alpha(\theta - \theta^*)} + 2\frac{\nu\nu^* \sin(\theta - \theta^*)\alpha'(\theta - \theta^*)}{\alpha(\theta - \theta^*)^2} \right. \\ & \left. + \frac{(1 - \nu\nu^* \cos(\theta - \theta^*))\alpha''(\theta - \theta^*)}{\alpha(\theta - \theta^*)^2} - 2\frac{(1 - \nu\nu^* \cos(\theta - \theta^*))\alpha'(\theta - \theta^*)^2}{\alpha(\theta - \theta^*)^3} \right) \end{aligned} \quad (80)$$

At optimality ( $\theta = \theta^*$  and  $\nu = \nu^*$ ), we have  $\alpha(0) = (1 - \nu^2)^2$ ,  $\alpha'(0) = 0$  and  $\alpha''(0) = 2\nu^2$ , so that

$$\frac{d^2L_t}{d\theta^2} = \frac{\nu^2(1 + \nu^2)}{(1 - \nu^2)^2}. \quad (81)$$

The optimal parametrization thus has to satisfy

$$\theta'(\omega_\theta) = \frac{1 - \nu^2}{\nu\sqrt{1 + \nu^2}}, \quad (82)$$

that is

$$\theta(\omega_\theta) = \omega_\theta \frac{1 - \nu^2}{\nu\sqrt{1 + \nu^2}} \quad (83)$$

There are two things we can remark:

- First, the parametrization that we derived for the general case in Section A.3.2, which additionally ignored the dependence of  $\gamma$  on  $\lambda$ , is relatively accurate. The only difference is the apparition of the extra  $\nu$  term, which becomes insignificant in the long memory limit  $\nu \rightarrow 1$ .
- Second, the optimal  $\theta$  parametrization has to be a function of  $\nu$ , and thus  $\omega_\nu$ , so the differential equation  $\nu$  needs to satisfy changes. Yet, this considerably simplifies the calculation and there is no simple solution to that problem. One could still argue that the initial choice we made, that is to use a polar parametrization, is the issue. It could be, but most practical models end up using that choice so highlighting the limitations of this choice has important practical consequences.

In the rest of this section, we ignore the dependency of  $\theta$  on  $\nu$ , and consider the optimal parametrization in this setting to be

$$\nu(\omega_\nu^{\text{opt}}) = \tanh(\omega_\nu^{\text{opt}}) \quad (84)$$

$$\theta(\omega_\theta^{\text{opt}}) = \omega_\theta^{\text{opt}} \frac{1 - \nu^2}{\nu\sqrt{1 + \nu^2}}. \quad (85)$$

### B.1.3 Visualization of the effect of input normalization and reparametrization

We now visualize the effect of input normalization and reparametrization on the loss landscape. We focus on two such reparametrizations:

- the one used in the LRU [20, 22] with  $\gamma(\lambda) = \sqrt{1 - \lambda^2}$ ,  $\nu = \exp(-\exp(\omega_\nu^{\text{exp}}))$  and  $\theta = \exp(\omega_\theta^{\text{exp}})$ .
- the optimal one we derived in the previous Section (c.f. Equations 84 and 85), which is tailored to this specific setting.

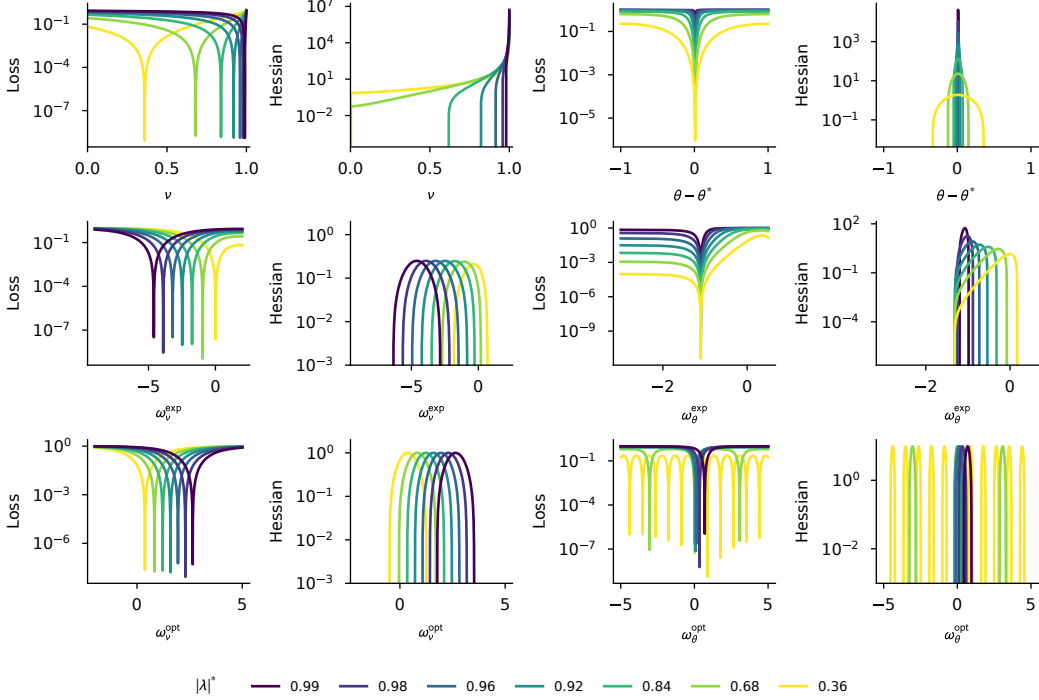


Figure 6: **Visualization of the loss landscape with input normalization, in the teacher and the student, for different parametrizations.** The teacher satisfies  $\lambda^* = |\lambda^*| \exp(i\pi/100)$ , for different  $|\lambda^*|$  values. The first two columns correspond to students with correct angle  $\theta = \theta^*$  but wrong absolute value  $\nu$  and the last two columns to students with correct absolute value  $\nu = |\lambda^*|$  but wrong angle. When we fix one variable, we ignore how it affects the loss for the Hessian calculation. Each line corresponds to a different parametrization: the first line uses a polar parametrization ( $\lambda = \nu \exp(i\theta)$ ), the second line uses the double exponential parametrization used in the LRU (exp) and the third one is the optimal parametrization for that task (tanh). Overall, both reparametrizations enable to control the explosion of the Hessian. However, the size of basins of attraction around optimality, or their number, shrinks as  $|\lambda^*|$  goes to 1 for the angle, but not for the absolute value, highlighting how difficult learning the angle can be.

#### B.1.4 Learning the angle is difficult in practice: an example

We use this one-dimensional teacher-student setting to test whether having a parametrization that avoids exploding behaviors at optimality, such as the one we derived in Section B.1.2, facilitates learning. Figure 6 already hints towards the fact the basin of attraction of the global minima is either extremely narrow or that their number decreases as longer memories are considered, making learning more tedious. Figure 7 confirms it. In this figure, we plot the learning dynamics obtained using the Adam optimizer with a learning rate of  $10^{-3}$  for 50k steps, starting from  $\lambda_0 = 0.99 \exp(i\pi/4)$ . We consider three different parametrizations of the angle:

$$\theta(\omega_\theta^{\text{polar}}) = \omega_\theta^{\text{polar}} \quad (86)$$

$$\theta(\omega_\theta^{\text{exp}}) = \log(\omega_\theta^{\text{exp}}) \quad (87)$$

$$\theta(\omega_\theta^{\text{opt}}) = \frac{(1 - \nu^2)}{\nu\sqrt{1 + \nu^2}} \omega_\theta. \quad (88)$$

The first one does not reparametrize the angle, the second one is the one used in the LRU and the third one is the optimal one we derived above. We use  $\nu = \tanh(\omega_\nu)$  to parametrize the magnitude in the three cases. We set  $\lambda^*$  to  $\lambda^* = 0.99 \exp(i\pi/100)$ . The  $\theta$  landscape when  $\nu$  is correct therefore corresponds to the ones plotted in the last two columns of Figure 6. This example shows that efforts to reduce the sharpness of the loss at optimality, as done in the last parametrization, inevitably make the loss flatter elsewhere and optimization impossible.



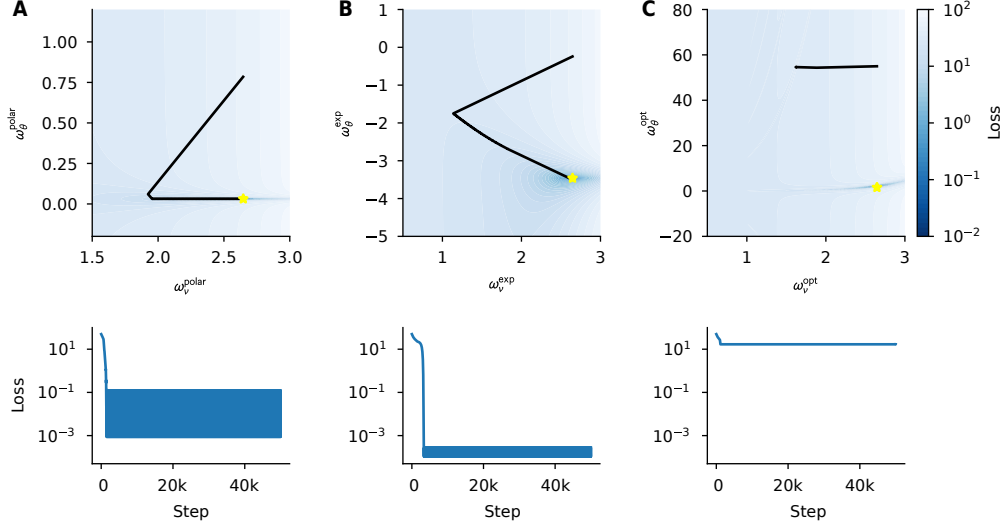


Figure 7: **Learning the angle is difficult, even in a simple one-dimensional task.** The target  $\lambda$  value is equal to  $\lambda^* = 0.99 \exp(i\pi/100)$  and is plotted in yellow. The black lines correspond to the Adam learning dynamics. **A.** When the angle is not reparametrized ( $\theta = \omega_\theta$ ), the loss landscape is extremely sharp in the  $\omega_\theta$  direction, but Adam compensates for it. **B.** When the angle is parametrized exponentially ( $\theta = \exp(\omega_\theta)$ ), the loss landscape becomes smoother. However, this only hold when the considered angles are small enough, as the exponential parametrization does not bring extra granularity elsewhere. **C.** When reparametrizing the angle to reduce the gradient explosion as  $|\lambda| \rightarrow 1$ , the loss becomes extremely tricky to navigate. The parameters are first attracted to a nearby valley, which is flat on the  $\omega_\theta$  direction and only indirectly connected to the global minimum. Such a reparametrization thus hinders optimization far away from optimality. See Section B.1.4 for more detail.

## B.2 Structure of the Hessian at optimality

In Section 4, we argue that the Hessian at optimality is an important object to understand the learning dynamics in the linear teacher-student task we consider. We here provide some theoretical analysis of its structure in the complex diagonal setting, that is we consider a recurrent network of the form

$$h_{t+1} = \lambda \odot h_t + b x_t \quad (89)$$

$$y_t = \text{Re}[c^\top h_t] + d x_t. \quad (90)$$

with  $\lambda, b$  and  $c$  complex vectors of size  $n$ , with  $n$  the number of hidden neurons, and  $d$  a scalar. We additionally take the loss to be the mean-square error, which is also the one we use in our numerical experiments. Note that, as in our theoretical analysis of Section 2, we consider infinitely long sequences and wide-sense stationary inputs.

Recall that the Hessian of the loss is equal to

$$\frac{d^2 L}{d\theta^2} = \sum_t \mathbb{E}_x \left[ \frac{dh_t}{d\theta} \frac{\partial^2 L_t}{\partial h_t^2} \frac{dh_t^\top}{d\theta} + \frac{\partial L_t}{\partial h_t} \frac{d^2 h_t}{d\theta^2} \right]. \quad (91)$$

At optimality, only the first term remains, as  $\partial_{h_t} L_t$  is 0 for all data points. Given that we have shown earlier, e.g. in Section A.2, that the most sensitive parameters to learn are the recurrent ones  $\lambda$ , we focus on the Hessian with respect to these parameters in the following.

### B.2.1 Hessian for complex-valued variables

Before delving into more specific calculations, we make a few remarks on how to deal the Hessian when having complex-valued parameters. We will mostly leverage the fact that the loss  $L$  is real-valued.

Before that, we recall a few facts about Wirtinger derivatives:

– For  $f(z)$  a complex-valued function of  $z$ , the Wirtinger derivatives are defined as:

$$\frac{df}{dz} = \frac{1}{2} \left( \frac{d\text{Re}[f]}{d\text{Re}[z]} - i \frac{d\text{Im}[f]}{d\text{Im}[z]} \right) \quad (92)$$

$$\frac{df}{d\bar{z}} = \frac{1}{2} \left( \frac{d\text{Re}[f]}{d\text{Re}[z]} + i \frac{d\text{Im}[f]}{d\text{Im}[z]} \right). \quad (93)$$

– We have

$$\frac{df}{dz} = \overline{\frac{df}{d\bar{z}}}. \quad (94)$$

– Leveraging the fact that  $L$  is real-valued so that  $\bar{L} = L$ , we have

$$\frac{d^2L}{d\lambda^2} = \frac{d}{d\lambda} \left[ \frac{dL}{d\lambda} \right]^\top \quad (95)$$

$$= \frac{d}{d\lambda} \left[ \overline{\frac{dL}{d\lambda}} \right] \quad (96)$$

$$= \frac{d^2\bar{L}}{d\bar{\lambda}^2} \quad (97)$$

and, similarly,  $d_\lambda d_{\bar{\lambda}} L = \overline{d_{\bar{\lambda}} d_\lambda L}$ . Second derivatives are symmetric, so we additionally have  $d_\lambda d_{\bar{\lambda}} L = d_{\bar{\lambda}} d_\lambda L^\top$ , which means that the complex Hessian is a Hermitian matrix.

Taken all together, this shows that the full complex Hessian, which contains all cross derivatives, has a similar structure to the real case.

## B.2.2 Hessian with respect to the recurrent eigenvalues

In this section, we compute the full complex Hessian with respect to the recurrent eigenvalue  $\lambda$  and defer the analysis of reparametrization to the next section.

First, let us remark that

$$\frac{dL_t}{d\lambda} = \frac{\partial L_t}{\partial y_t} c^\top \frac{dh_t}{d\lambda} \quad (98)$$

$$(99)$$

so that

$$\frac{d^2L_t}{d\lambda^2} = \frac{d}{d\lambda} \left[ \frac{dh_t}{d\lambda} c^\top \frac{\partial L_t}{\partial y_t} \right]^\top \quad (100)$$

$$= \frac{d^2h_t}{d\lambda^2} c^\top \frac{\partial L_t}{\partial y_t} + \frac{dh_t}{d\lambda} c^\top \frac{\partial^2 L_t}{\partial y_t^2} c^\top \frac{dh_t}{d\lambda} \quad (101)$$

We assumed that we are at optimality so that the network perfectly fits the target trajectories and  $\partial_{y_t} L_t = 0$ . Additionally,  $L_t$  is the mean-squared error loss so that  $\partial_{y_t}^2 L_t = \text{Id}$ . It follows that

$$\left( \frac{d^2L_t}{d\lambda^2} \right)_{ij} = \left( \frac{dh_t}{d\lambda} c^\top \frac{dh_t}{d\lambda} \right)_{ij} \quad (102)$$

$$= \left( c^\top \frac{dh_t}{d\lambda} \right)_i \left( c^\top \frac{dh_t}{d\lambda} \right)_j \quad (103)$$

$$= c_i \frac{dh_{t,i}}{d\lambda_i} c_j \frac{dh_{t,j}}{d\lambda_j}. \quad (104)$$

In the last equation, we made use of the fact that the parameter  $\lambda_i$  only affects the hidden state  $h_{t,i}$  and not the others, so  $d_{\lambda_j} h_{t,i} = 0$  if  $i \neq j$ .

The previous calculation applied to one sequence, we now take the expectation over the data:

$$\frac{d^2L}{d\lambda^2} = (cc^\top) \odot \mathbb{E}_{x,y} \left[ \lim_{t \rightarrow \infty} \frac{dh_t}{d\lambda} \frac{dh_t}{d\lambda}^\top \right] \quad (105)$$

Note that we introduced a slight abuse of notation in the previous equation as  $d_\lambda h_t$  is in general a matrix. However, given that the hidden neurons are independent here due to the diagonal connectivity, it is effectively a vector, and we treat it that way. Let us now compute the expectation, using similar calculation techniques to the one we used in Section A.2:

$$\mathbb{E}_{x,y} \left[ \lim_{t \rightarrow \infty} \frac{dh_{t,i}}{d\lambda_i} \frac{dh_{t,j}}{d\lambda_j} \right] = \mathbb{E} \left[ \sum_{n,m \geq 0} n \lambda_i^{n-1} b_i x_{-n} m \lambda_j^{m-1} b_j x_{-m} \right] \quad (106)$$

$$= b_i b_j \mathbb{E} \left[ \sum_{n,m \geq 0} n \lambda_i^{n-1} x_{-n} m \lambda_j^{m-1} x_{-m} \right] \quad (107)$$

$$= b_i b_j \sum_{n,m \geq 0} n m \lambda_i^{n-1} \lambda_j^{m-1} R_x(n-m) \quad (108)$$

We can now remark that this quantity is very similar to the one we have encountered in Section A.2, up to the presence of  $b_i b_j$ , and can be simplified using Lemma 2. For conciseness, we note  $S(\lambda_i, \lambda_j)$  the right-hand side of the last equation without the  $b_i b_j$  factor. Putting this result back in the Hessian, we get

$$\frac{d^2L}{d\lambda_i d\lambda_j} = b_i b_j c_i c_j S(\lambda_i, \lambda_j) \quad (109)$$

To gain further intuition of the behavior of this quantity, we take  $R_x(\Delta) = \rho^{|\Delta|}$ ,  $\rho$  being a real number. A similar calculation to the one we did in Section A.2 gives

$$S(\lambda_i, \lambda_j) = \frac{(1-\rho)(1+\lambda_i \lambda_j) + \rho^2(1-\lambda_i \lambda_j)^3 + \rho(1-\rho)\lambda_i \lambda_j (\rho \lambda_i \lambda_j (1+\lambda_i \lambda_j) - 2\lambda_i - 2\lambda_j)}{(1-\lambda_i \lambda_j)^3 (1-\rho \lambda_i)^2 (1-\rho \lambda_j)^2} \quad (110)$$

This formula being still hard to grasp, we visualize the magnitude of  $S(\lambda_i, \lambda_j)$  on Figure 8. Interestingly, we observe this quantity is large when  $\lambda_i$  and  $\lambda_j$  are conjugate to each other and inputs are uncorrelated. However, as elements in the input sequence get more correlated ( $\rho \rightarrow 1$ ), this effect disappears and  $|S|$  increases as one of the two eigenvalue gets closer to 1 in the complex plane. In both cases, the effect gets amplified as the magnitude of the eigenvalue increases.

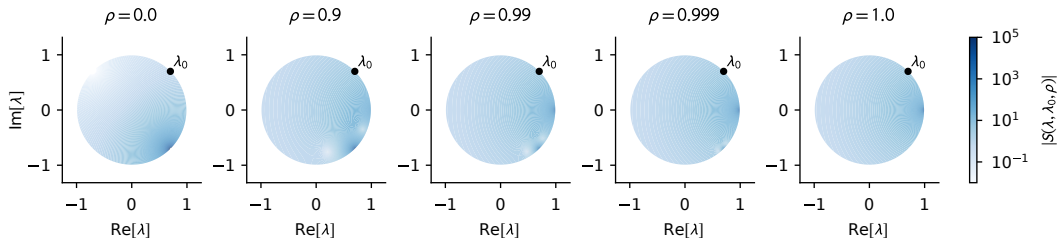


Figure 8: **Visualization of  $\lambda \mapsto |S(\lambda, \lambda_0)|$  for  $\lambda_0 = 0.99 \exp(i\pi/4)$ .** This term measures how "similar" eigenvalues are in the Hessian. When  $\rho = 0$ , eigenvalues are mostly "similar" when they are conjugate to each other. As  $\rho$  increases, this effect decreases and eigenvalues become more "similar" if one of them gets close to 1.

We also need to compute  $d_{\bar{\lambda}} d_\lambda L$  to get the full complex Hessian. Similarly to the previous calculation, we first have

$$\frac{dL_t}{d\bar{\lambda}} = \overline{\frac{dL_t}{d\lambda}} = \overline{\frac{\partial L_t}{\partial y_t} \bar{c}^\top} \frac{d\bar{h}_t}{d\bar{\lambda}} \quad (111)$$

It follows that

$$\frac{d^2 L}{d\lambda_i d\bar{\lambda}_j} = \mathbb{E} \left[ \frac{d\overline{h_{t,j}}}{d\lambda_j} \bar{c}_j c_i \frac{dh_{t,i}}{d\lambda_i} \right] \quad (112)$$

$$= c_i \bar{c}_j b_i \bar{b}_j S(\lambda_i, \bar{\lambda}_j). \quad (113)$$

Using the symmetry with the complex Hessian matrix, we now have all its components.

### B.2.3 Hessian for different parametrizations

So far, we have computed the complex Hessian, which is not of direct use as we end up optimizing real numbers in practice. Here, we study the impact of different parametrizations of  $\lambda$  on the Hessian. Given that this parametrization only affects  $\lambda$  and not the other parameters in the network and that we only consider the Hessian at optimality here, computing the Hessian of those parameters reduces to left and right multiplying the Hessian by derivatives of  $\lambda$  and  $\bar{\lambda}$  with respect to these parameters. For future reference, we introduce

$$H_{ij}^\lambda := \begin{pmatrix} \frac{d^2 L}{d\lambda_i d\lambda_j} & \frac{d^2 L}{d\lambda_i d\bar{\lambda}_j} \\ \frac{d^2 L}{d\bar{\lambda}_i d\lambda_j} & \frac{d^2 L}{d\bar{\lambda}_i d\bar{\lambda}_j} \end{pmatrix} = \begin{pmatrix} A_{ij} & B_{ij} \\ \bar{B}_{ij} & \bar{A}_{ij} \end{pmatrix} \quad (114)$$

with  $A_{ij} := b_i b_j c_i c_j S(\lambda_i, \lambda_j)$  and  $B_{ij} = b_i \bar{b}_j c_i \bar{c}_j S(\lambda_i, \bar{\lambda}_j)$ .

**Real-imaginary parametrization:**  $\lambda = \omega_{\text{re}} + \omega_{\text{im}}$ . We aim at computing the matrix

$$H_{ij}^{\text{RI}} := \begin{pmatrix} \frac{d^2 L}{d\omega_{\text{re},i} d\omega_{\text{re},j}} & \frac{d^2 L}{d\omega_{\text{re},i} d\omega_{\text{im},j}} \\ \frac{d^2 L}{d\omega_{\text{im},i} d\omega_{\text{re},j}} & \frac{d^2 L}{d\omega_{\text{im},i} d\omega_{\text{im},j}} \end{pmatrix}, \quad (115)$$

which is the building block to compute the full Hessian. First, let us remark that  $d_{\omega_{\text{re},i}} \lambda_i = 1/2$ ,  $d_{\omega_{\text{re},i}} \bar{\lambda}_i = 1/2$ ,  $d_{\omega_{\text{im},i}} \lambda_i = i/2$  and  $d_{\omega_{\text{im},i}} \bar{\lambda}_i = -i/2$ . It follows that

$$\frac{d^2 L}{d\omega_{\text{re},i} d\omega_{\text{re},j}} = (d_{\omega_{\text{re},j}} \lambda_j \quad d_{\omega_{\text{re},j}} \bar{\lambda}_j) H_{ij}^\lambda (d_{\omega_{\text{re},i}} \lambda_i \quad d_{\omega_{\text{re},i}} \bar{\lambda}_i)^\top \quad (116)$$

$$= \frac{1}{4} (1 \quad 1) H_{ij}^\lambda (1 \quad 1)^\top \quad (117)$$

$$= \frac{1}{2} (\text{Re}[A_{ij}] + \text{Re}[B_{ij}]). \quad (118)$$

Once again we emphasize that the first line only holds as we are at optimality. Similar calculations give the rest of the elements of  $H_{ij}^{\text{RI}}$ :

$$H_{ij}^{\text{RI}} := \frac{1}{2} \begin{pmatrix} \text{Re}[A_{ij} + B_{ij}] & \text{Im}[-A_{ij} + B_{ij}] \\ \text{Im}[-A_{ij} - B_{ij}] & \text{Re}[-A_{ij} + B_{ij}] \end{pmatrix}. \quad (119)$$

Given the intuition we gained on the structure of  $S$  previously, and the fact that  $A_{ij} \propto S(\lambda_i, \lambda_j)$  and  $B_{ij} \propto S(\lambda_i, \bar{\lambda}_j)$ , we know that this block will have large components if the two corresponding eigenvalues are conjugate of each other or aligned to each other, or if one of them is close to 1.

One other quantity that we can calculate is the trace of the Hessian  $H^{\text{RI}}$ , which is equal to the sum of its eigenvalues. Note that this does not correspond to the eigenvalues of the full Hessian matrix, as it additionally contains entries for other parameters. Yet it already provides some idea of how large the Hessian will be, as the value of this trace appears in the value of the full trace. We have

$$\text{Tr}[H^{\text{RI}}] = \sum_i \frac{1}{2} (\text{Re}[A_{ii} + B_{ii}] + \text{Re}[-A_{ii} + B_{ii}]) \quad (120)$$

$$= \sum_i \text{Re}[B_{ii}] \quad (121)$$

$$= \sum_i |b_i|^2 |c_i|^2 S(\lambda_i, \bar{\lambda}_i) \quad (122)$$

where we used that  $S(\lambda_i, \bar{\lambda}_i)$  is real-valued in the last line. As a side note, this formula partly justifies why studying the expected squared magnitude of  $d_\lambda h_t$  in Section 2 makes general sense, as

$$\mathbb{E} \left[ \left| \frac{dh_{t,i}}{d\theta} \right|^2 \right] = |b_i|^2 S(\lambda_i, \bar{\lambda}_i). \quad (123)$$

**Magnitude-angle parametrization:**  $\lambda = \nu(\omega_\nu) \exp(i\theta(\omega_\theta))$ . The calculations for this parametrization are similar to the previous one, with the following differences:

$$\frac{d\lambda}{d\omega_\nu} = \frac{\nu'(\omega_\nu) \exp(i\theta(\omega_\theta))}{2} \quad (124)$$

$$\frac{d\bar{\lambda}}{d\omega_\nu} = \frac{\nu'(\omega_\nu) \exp(-i\theta(\omega_\theta))}{2} \quad (125)$$

$$\frac{d\lambda}{d\omega_\theta} = \frac{i\nu(\omega_\nu)\theta'(\omega_\theta) \exp(i\theta(\omega_\theta))}{2} \quad (126)$$

$$\frac{d\bar{\lambda}}{d\omega_\theta} = -\frac{i\nu(\omega_\nu)\theta'(\omega_\theta) \exp(-i\theta(\omega_\theta))}{2}. \quad (127)$$

After some calculations we obtain

$$\frac{d^2 L}{d\omega_{\nu,i} d\omega_{\nu,j}} = \frac{\nu'(\omega_{\nu,i})\nu'(\omega_{\nu,j})}{2} \text{Re}[e^{i(\theta(\omega_{\theta,i})+\theta(\omega_{\theta,j}))} A_{ij} + e^{i(\theta(\omega_{\theta,i})-\theta(\omega_{\theta,j}))} B_{ij}] \quad (128)$$

$$\frac{d^2 L}{d\omega_{\nu,i} d\omega_{\theta,j}} = \frac{\nu'(\omega_{\nu,i})\nu(\omega_{\nu,j})\theta'(\omega_{\theta,j})}{2} \text{Im}[-e^{i(\theta(\omega_{\theta,i})+\theta(\omega_{\theta,j}))} A_{ij} + e^{i(\theta(\omega_{\theta,i})-\theta(\omega_{\theta,j}))} B_{ij}] \quad (129)$$

$$\frac{d^2 L}{d\omega_{\theta,i} d\omega_{\nu,j}} = \frac{\nu(\omega_{\nu,i})\theta'(\omega_{\theta,i})\nu'(\omega_{\nu,j})}{2} \text{Im}[-e^{i(\theta(\omega_{\theta,i})-\theta(\omega_{\theta,j}))} A_{ij} + e^{i(\theta(\omega_{\theta,i})-\theta(\omega_{\theta,j}))} B_{ij}] \quad (130)$$

$$\frac{d^2 L}{d\omega_{\theta,i} d\omega_{\theta,j}} = \frac{\nu(\omega_{\theta,i})\theta'(\omega_{\theta,i})\nu(\omega_{\theta,j})\theta'(\omega_{\theta,j})}{2} \text{Re}[-e^{i(\theta(\omega_{\theta,i})+\theta(\omega_{\theta,j}))} A_{ij} + e^{i(\theta(\omega_{\theta,i})-\theta(\omega_{\theta,j}))} B_{ij}] \quad (131)$$

### B.3 Experimental details

We recall the setup we consider in Section 4:

$$h_{t+1} = Ah_t + Bx_{t+1} \text{ and } y_t = Ch_t + Dx_t. \quad (132)$$

with  $h_t \in \mathbb{R}^n$ ,  $x_t \in \mathbb{R}$  drawn i.i.d. from  $\mathcal{N}(0, 1)$ ,  $A \in \mathbb{R}^{n \times n}$ ,  $B \in \mathbb{R}^{n \times 1}$ ,  $C \in \mathbb{R}^{1 \times n}$  and  $D \in \mathbb{R}^{1 \times 1}$ . We draw  $B$ ,  $C$  and  $D$  from truncated normal distributions with fan\_in scaling. We draw each entry of  $A$  from  $\mathcal{N}(0, 1/\sqrt{n})$  and then apply the following postprocessing to it: First we complex diagonalize  $A$ , which we can do almost surely. Note  $\lambda$  its eigenvalues. We then transform them according to

$$\lambda \leftarrow (\nu + (1 - \nu) \tanh(|\lambda|)) \exp\left(i \frac{\text{angle}(\lambda)}{\pi} \theta_0\right) \quad (133)$$

with  $\nu$  and  $\theta_0$  two scalars that we control. This transformation has several benefits: we are guaranteed that the magnitude of  $\lambda$  is within  $[\nu, 1]$  (and in  $[\nu, \nu + (1 - \nu) \tanh(1)]$  in the limit  $n \rightarrow \infty$  as the eigenvalues of  $A$  stay within the unit circle in that limit), and conjugate pairs of eigenvalues remain conjugate. This last point ensures that the resulting matrix remains real without having to change the eigenvectors.

We implement our experiments in JAX [62], using the default Flax [63] implementation of RNNs and the LRU implementation of Zucchet et al. [64]. We initialize RNNs in the same way we initialized the teacher, and initialize the eigenvalues of the LRU and other complex-valued networks with magnitude in  $[\nu, 1]$  and angle within  $[-\theta_0, \theta_0]$ .

Given that we are interested in the optimization properties of the different architectures, we only report training losses and do not perform any cross validation.

Here are additional details related to the different figures:

- **Figure 3:** see Tables 1 and 2.
- **Figure 4:** for panels A and B, we use  $\nu = 0.99$  and draw  $A$  in a slightly different manner to the one described above (we directly draw the eigenvalues and eigenvectors so that we have two pairs of complex eigenvalues). We use automatic differentiation to compute the Hessian. For panels C and D, we use the same setup as described in Table 2, but keep the learning rate constant over the course of learning. We report the effective learning rate at the end of learning.

	RNN	LRU
Batch size		128
Sequence length		300
Hidden neurons (teacher)		10
Input / output dimension		1
$\nu$	{0.32, 0.68, 0.84, 0.92, 0.96, 0.98, 0.99}	
$\theta_0$	$\pi$	
Hidden neurons (student)		64
log learning rate	$[-5, -4.5, -4, -3.5, -3, -2.5]$	$[-2.5, -2, -1.5, -1, -0.5]$
Optimizer (schedule)	Adam (cosine)	
Initialization	$[\nu \text{ teacher}, \nu = 0]$	$\nu \text{ teacher}$
Number iterations		10k
Seeds		10

Table 1: **Experimental details for Figure 3.A.** We use  $[\dots]$  to denote hyperparameters that were scanned over with grid search and  $\{\dots\}$  to denote the variables of interest for the figure. We chose the learning rates for the two architectures on preliminary scans and verified that non of the extreme learning rates were optimal in the final scan. For the RNN, we found that initializing with  $\nu = 0$  gave better results than initializing with the same distribution the teacher has, so we included this choice in the scan.

	RNN / BLOCK DIAG. RNN	COMPLEX DIAG. RNN / LRU
Batch size		128
Sequence length		300
Hidden neurons (teacher)		10
Input / output dimension		1
$\nu$		0.99
$\theta_0$		$\pi$
Hidden neurons (student)	64 / 64 and 128	64
log learning rate	$[-5, -4.5, -4, -3.5, -3, -2.5]$	$[-2.5, -2, -1.5, -1, -0.5]$
Optimizer (schedule)	Adam (cosine)	
Initialization	$[\nu \text{ teacher}, \nu = 0]$	$\nu \text{ teacher}$
Number iterations		10k
Seeds		10

Table 2: **Experimental details for Figure 3.B.** We use  $[\dots]$  to denote hyperparameters that were scanned over with grid search and  $\{\dots\}$  to denote the variables of interest for the figure. We chose the learning rates for the two architecture types on preliminary scans and verified that non of the extreme learning rates were optimal in the final scan. For the RNN, we found that initializing with  $\nu = 0$  gave better results than initializing with the same distribution the teacher has, so we included this choice in the scan. For the RNNs, we used 64 neurons for the "RNN" entry, 64 for the "block diagonal" one, and 128 for the "more neurons" one.

- **Figure 10:** for panels A, B and C, we draw the magnitude and angle of 10  $\lambda$  independently, uniformly in  $[\nu, \frac{1+\nu}{2}]$  and  $[-\theta_0, \theta_0]$ . Importantly, this means that there are no conjugate pairs, which leads to more diagonal Hessian matrices at optimality than in Figure 4. For panel D, see Table 3.

As a rule of thumb, each LRU (or complex-valued diagonal network) experiment takes 3 minutes on a consumer-scale GPU (NVIDIA GeForce RTX 3070) and each RNN experiment takes 10 minutes on a CPU. The scans behind the results reported in the different figures require on the order of few hundreds run each. Including our preliminary exploration, the results we report in this section required 30 days of compute, one third of it on GPUs and two thirds on CPUs.

	RNN	COMPLEX DIAG. RNN / LRU
Batch size		128
Sequence length		300
Hidden neurons (teacher)		10
Input / output dimension		1
$\nu$		0.99
$\log(\theta_0/\pi)$		$\{-2, -1.5, -1, -0.5, 0\}$
Hidden neurons (student)		64
log learning rate	$[-4.5, -4, -3.5, -3]$	$[-3.5, -3, \dots, -0.5, 0]$
Optimizer (schedule)		Adam (cosine)
Initialization	$[\nu \text{ teacher}, \nu = 0] + \theta \text{ teacher}$	$\nu \text{ teacher} + \theta \text{ teacher}$
Number iterations		10k
Seeds		10

Table 3: **Experimental details for Figure 10.** We use  $[\dots]$  to denote hyperparameters that were scanned over with grid search and  $\{\dots\}$  to denote the variables of interest for the figure. We chose the learning rates for the two architectures on preliminary scans and verified that non of the extreme learning rates were optimal in the final scan. For the RNN, we found that initializing with  $\nu = 0$  gave better results than initializing with the same distribution the teacher has, so we included this choice in the scan.

## B.4 Additional analyses

### B.4.1 Structure of the loss landscape for LRUs

In the main text, we only provide an analysis of the loss landscape for the fully connected linear recurrent neural network and its complex-valued diagonal counterpart. We here complete this result by performing the same analysis for the LRU.

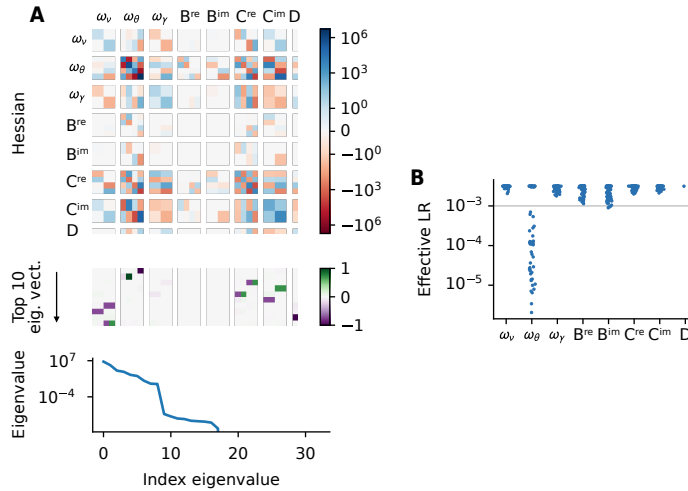


Figure 9: **Equivalent of Figure 4 for the LRU.** The exponential parametrization of the magnitude  $\nu = \exp(-\exp(\omega_\nu))$  efficiently mitigates the Hessian explosion but not the one of the angle  $\theta = \exp(\omega_\theta)$ , consistently with the theoretical and empirical evidence we have accumulated so far.

### B.4.2 Concentrating eigenvalue distributions

The goal of this experiment is to better understand how the concentration of eigenvalues  $\lambda$  affect the learning dynamics. For fully connected RNNs, there is no reason to expect a major change in behavior. However, it is different for diagonal RNNs. The theoretical analysis we have done in Section B.2 provides us with the following insights. When the elements in the input sequence

are uncorrelated, as it is the case here, the entries in the Hessian corresponding to two different eigenvalues increase if they are aligned or conjugate to each other, and if their magnitude is large. We therefore expect that, as the interval on which the angle of the teacher’s eigenvalues shrinks ( $\theta_0 \rightarrow 0$ ), those eigenvalues will be more likely to be "similar" to each other. This results in large non-diagonal terms, as we confirm in Figure 10.A, B and C. The LRU suffers less from this problem thanks to its reparametrization, which reduces the overall magnitude of Hessian entries related to the magnitude, and partly the one of angle parameters (when it is a small positive number). As a consequence, the performance between these two architectures increases as  $\theta_0 \rightarrow 0$ , as seen on Figure 10.D.

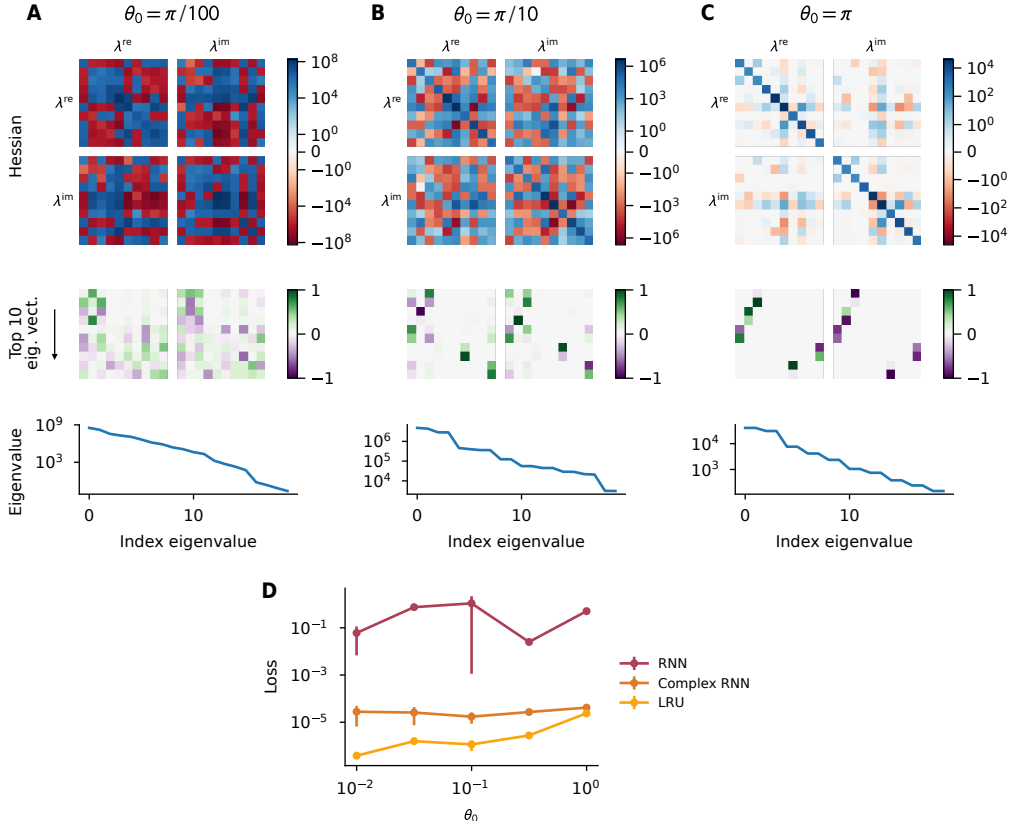


Figure 10: **Concentrating eigenvalues make the Hessian less diagonal ( $\theta_0 \rightarrow 0$ ) and consequently increases the gap between the LRU and the complex-valued diagonal RNN.** A, B, C. Hessian of the loss with respect to the  $\lambda$  parameters in the complex-valued diagonal RNN. The Hessian is computed through the theoretical formula of Equation 119; computing it numerically marginally affects the results. Consistently with the intuition we developed in Section B.2, concentrating the eigenvalues affect the structure of the loss landscape. It makes the Hessian at optimality less diagonal and Adam cannot efficiently compensate it. The LRU does not suffer as much from this problem, and the gap between the two architecture widens as  $\theta_0 \rightarrow 0$ .

## C Signal propagation in deep recurrent neural networks at initialization

### C.1 Experimental setup

We here detail the experimental setup we used in Section 5. We take 1024 random sequences from the Wikipedia dataset [65] and pass it through the BERT [66] tokenizer and embedding layer. This provides us with a dataset of 1024 examples, we cut their length at 512. Each embedding has 724 features.

We consider networks with 4 blocks of the following structure: a recurrent layer, a non-linearity, a gated linear unit [57, GLU] and a skip connection. By default, we do not use any normalization layer,



but when we do, as in Figure 5.C, we include one normalization layer before the recurrent layer and another one before the GLU. All the layers involved use 256 neurons. We additionally add a linear encoder at the beginning of the network, and a linear decoder at the end.

In Figure 5 we vary  $\nu$ , which controls the magnitude of the eigenvalues of the recurrent Jacobian. More precisely, we sample those magnitudes in the interval  $[\nu, (1 + \nu)/2]$ . For the complex-valued diagonal RNN and the LRU, we use the LRU initialization. For the LSTM, we use the chrono initialization of Tallec and Ollivier [29]: it initializes the bias of the forget and input gates such that, when the input  $x$  and the hidden state  $h$  are equal to 0, the time constant associated to  $f$  is uniformly sampled from  $[\frac{1}{1-\nu}, \frac{2}{1-\nu}]$  and the input gate  $i$  is equal to  $1 - f$ .

The loss that we use is a next-token mean-squared error, that is

$$L_t = \frac{1}{2} \|\hat{x}_t(x_{1:t-1}) - x_t\|^2 \quad (134)$$

with  $\hat{x}_t(x_{1:t-1})$  the prediction of the network. The quantities reported in Figure 5 are the average squared value the hidden state or the gradient takes. The average is taken over all the sequences, but also over all neurons / parameters and over all time steps. Gradients are computed on batches of size 8.